Neuron
Article

Whole-Brain Mapping of Direct Inputs to Midbrain Dopamine Neurons

Mitsuko Watabe-Uchida,[1] Lisa Zhu,[1] Sachie K. Ogawa,[1] Archana Vamanrao,[1] and Naoshige Uchida[1,*]
[1]Center for Brain Science, Department of Molecular and Cellular Biology, Harvard University, 16 Divinity Avenue, Cambridge, MA 02138, USA
*Correspondence: uchida@mcb.harvard.edu
DOI 10.1016/j.neuron.2012.03.017

SUMMARY

Recent studies indicate that dopamine neurons in the ventral tegmental area (VTA) and substantia nigra pars compacta (SNc) convey distinct signals. To explore this difference, we comprehensively identified each area's monosynaptic inputs using the rabies virus. We show that dopamine neurons in both areas integrate inputs from a more diverse collection of areas than previously thought, including autonomic, motor, and somatosensory areas. SNc and VTA dopamine neurons receive contrasting excitatory inputs: the former from the somatosensory/motor cortex and subthalamic nucleus, which may explain their short-latency responses to salient events; and the latter from the lateral hypothalamus, which may explain their involvement in value coding. We demonstrate that neurons in the striatum that project directly to dopamine neurons form patches in both the dorsal and ventral striatum, whereas those projecting to GABAergic neurons are distributed in the matrix compartment. Neuron-type-specific connectivity lays a foundation for studying how dopamine neurons compute outputs.

INTRODUCTION

A central goal of neuroscience is to understand brain function in terms of interactions among a network of diverse types of neurons. A critical step is to understand the inputs and outputs of a given type of neuron in an intact network. Electrophysiological and optical imaging techniques have advanced our understanding of outputs, but our progress in understanding the nature of inputs has been slow. Establishing methods to efficiently identify inputs to a given type of neuron will facilitate our understanding of how neurons communicate.

Dopamine neurons in the ventral tegmental area (VTA) and substantia nigra pars compacta (SNc) play pivotal roles in various brain functions including motivation, reinforcement learning, and motor control (Cohen et al., 2012; Ikemoto, 2007; Redgrave and Gurney, 2006; Schultz, 2007; Wise, 2004). Electrophysiological studies have shown that dopamine neurons are activated phasically (100–500 ms) by unpredicted reward or sensory cues that predict reward (Bromberg-Martin et al., 2010; Schultz et al., 1997). In contrast, they do not respond to fully predicted reward, and their activity is transiently suppressed by negative outcomes (e.g., when a predicted reward is omitted or the animal expects or receives negative outcomes). Thus, dopamine neurons appear to calculate the difference between the expected and actual reward (i.e., reward prediction errors).

Reward prediction error may not be the only function of dopamine neurons, however. For example, several studies have suggested that dopamine neurons are activated by noxious stimuli (Brischoux et al., 2009; Joshua et al., 2008; Redgrave and Gurney, 2006). Indeed, a recent study in nonhuman primates found at least two types of dopamine neurons, saliency coding and value coding, that are activated and inhibited, respectively, by aversive events (Matsumoto and Hikosaka, 2009). Importantly, saliency-coding dopamine neurons were found preferentially in the dorsolateral part of the midbrain dopamine nuclei (i.e., mainly SNc) while reward-value-coding dopamine neurons were found in the more ventromedial part (i.e., mainly VTA). Furthermore, responses in SNc were generally earlier than those in VTA. These findings raise the possibility that inputs encoding noxious stimuli or saliency specifically innervate SNc dopamine neurons. Although efforts have been made to identify the sources of such inputs, they remain unidentified (Bromberg-Martin et al., 2010; Coizet et al., 2010; Dommett et al., 2005; Jhou et al., 2009; Matsumoto and Hikosaka, 2007). More generally, although the aforementioned findings indicate that dopamine neurons integrate diverse kinds of information, the mechanisms by which the firing of dopamine neurons is regulated in a behavioral context remain largely unknown (Bromberg-Martin et al., 2010; Lee and Tepper, 2009; Sesack and Grace, 2010).

A critical step toward understanding the aforementioned questions is to know what kinds of inputs dopamine neurons in the VTA and SNc receive. Circuit-tracing experiments have been performed to address this question (Geisler et al., 2007; Geisler and Zahm, 2005; Graybiel and Ragsdale, 1979; Phillipson, 1979; Sesack and Grace, 2010; Swanson, 2000; Zahm et al., 2011), but limitations of conventional tracing methods have hampered a full understanding of inputs to dopamine neurons. For example, conventional tracing cannot distinguish between dopaminergic and nondopaminergic cells (e.g., GABAergic neurons). Furthermore, SNc dopamine neurons form a thin layer and are heavily interconnected with the neighboring substantia nigra pars reticulata (SNr), and conventional tracing might label inputs to SNr in addition to SNc. Finally, there are many axons of passage through or near these structures, which may take up tracers nonspecifically. Thus, it is unclear

whether neurons in a given area project to VTA or SNc and whether they actually make synaptic contacts with dopamine neurons.

Electron microscopy can resolve several of these issues (e.g., Bolam and Smith, 1990; Carr and Sesack, 2000; Omelchenko et al., 2009; Omelchenko and Sesack, 2010; Somogyi et al., 1981), but this technique is not suitable for a comprehensive identification of inputs. Another approach is to combine anatomical methods with electrophysiological or optogenetic techniques (Chuhma et al., 2011; Collingridge and Davies, 1981; Grace and Bunney, 1985; Lee and Tepper, 2009; Xia et al., 2011). However, the validity of this approach has been called into question after these studies (Chuhma et al., 2011; Xia et al., 2011) failed to demonstrate well-accepted direct projections from striatum to dopamine neurons in the VTA and SNc (Bolam and Smith, 1990; Collingridge and Davies, 1981; Grace and Bunney, 1985; Lee and Tepper, 2009; Somogyi et al., 1981).

To resolve these methodological issues, we combined the Cre/loxP gene expression system (Gong et al., 2007) with rabies-virus-based transsynaptic retrograde tracing (Wickersham et al., 2007b) to comprehensively identify monosynaptic inputs to a genetically defined neural population (Haubensak et al., 2010; Miyamichi et al., 2011; Wall et al., 2010). This technique allowed us to identify the sources of monosynaptic inputs to VTA and SNc dopamine neurons in the entire brain. We then asked whether we can identify different sources of candidate excitatory inputs that may account for rapid activation of SNc dopamine neurons by salient events, in contrast to activation of VTA dopamine neurons by reward values, and whether there are indeed direct projections from the striatum to dopamine neurons. We show that SNc dopamine neurons receive relatively strong excitatory inputs from the somatosensory and motor cortices, as well as subthalamic nucleus (STh), whereas VTA dopamine neurons receive strong inputs from the lateral hypothalamus (LH). Furthermore, we show that neurons in the striatum project directly to VTA and SNc dopamine neurons, forming "patch" compartments in both the ventral striatum (VS) and dorsal striatum (DS).

RESULTS

Visualization of Monosynaptic Inputs to a Genetically Defined Population of Neurons Using Rabies Virus and cre/loxP Recombination System

We used the modified rabies virus SADΔG-GFP(EnvA), which has two key modifications that determine the specificity of its initial infection and transsynaptic spread (Wickersham et al., 2007b). First, this virus is pseudotyped with an avian virus envelope protein (EnvA) and therefore cannot infect mammalian cells. In mammalian brains, the initial infection thus occurs only when a host neuron is engineered to express a cognate receptor (e.g., TVA). Second, the gene for the rabies virus envelope glycoprotein (RG), which is required for transsynaptic spread, is replaced by the gene for a fluorescent marker (enhanced green fluorescent protein; EGFP). Transsynaptic transfer thus occurs only from neurons that exogenously express RG.

Our strategy was to express TVA and RG only in a genetically defined cell population (Haubensak et al., 2010; Miyamichi et al., 2011; Wall et al., 2010). Thus, we generated adeno-associated viruses (AAVs) that express either TVA or RG (AAV5-FLEX-TVA-mCherry and AAV8-FLEX-RG, respectively). We used the transmembrane type of the TVA receptor protein (TVA950) to generate a fusion protein with a red fluorescent protein (mCherry). TVA and RG proteins were expressed under the control of a high-specificity Cre/loxP recombination system (a modified Flex switch) and different promoters (EF-1α and CAG, respectively) (Figure 1A).

To visualize monosynaptic inputs to dopamine neurons, we injected AAV5-FLEX-TVA-mCherry and AAV8-FLEX-RG stereotaxically into VTA or SNc of transgenic mice that express Cre in dopamine neurons (dopamine transporter-Cre or DAT-Cre) (Bäckman et al., 2006). After 14 days, SADΔG-GFP(EnvA) was injected into the same area and the brain was analyzed after 7 days (Figure 1B). The whole brain was sectioned at 100 μm, and every third section was processed for further analysis. The starter cells were identified based on the coexpression of TVA-mCherry and EGFP (Figures 1C and 1H; Figure S1 available online). Coexpressing neurons were found only in the injected area, while EGFP-positive neurons outside the injected area did not express TVA-mCherry, indicating that they are transsynaptically labeled neurons. We found a large number of these transsynaptically labeled neurons (Figure 1D;$6.1 \times 10^3 \pm 4.2 \times 10^3$ neurons; mean ± SD, n = 12 mice), although the number of labeled neurons varied across animals, in part due to different injection volumes (Figures 1E and 1F). Nevertheless, the numbers of transsynaptically labeled neurons were roughly proportional to the numbers of starter neurons (Figure 1G).

To examine the specificity of tracing, we first repeated the aforementioned procedure in mice with no Cre expression (Figure 1D, right). This resulted in much smaller numbers of EGFP-labeled neurons both outside and near the injection site (87 ± 61 neurons outside VTA or SNc and 31 ± 21 neurons in VTA or SNc; mean ± SD) compared to the aforementioned result. This small degree of labeling was likely due to inevitable contamination of the unpseudotyped rabies virus that occurred during the viral preparation. Note that these numbers should be regarded as the upper bounds of nonspecific labeling, as some of the labeled neurons are likely dopamine neurons and their inputs. Next, to examine the specificity of the initial infection and to verify that the transsynaptic spread is under the tight control of RG expression, we repeated the experiment without AAV8-FLEX-RG in DAT-Cre mice. A larger number of labeled neurons were found at the injection site, and 97% of the labeled neurons coexpressed tyrosine hydroxylase, a marker for dopamine neurons. Furthermore, very few neurons were found outside the injection site. This result confirms that the TVA proteins were expressed specifically in Cre-expressing neurons and that transsynaptic spread did not occur without RG protein. Together, these results suggest that labeled neurons outside the injection site represent monosynaptic inputs to dopamine neurons, while the injection site contains a small number of nonspecifically labeled neurons that contributed very little labeling outside the injection site (~1.3%). In the following analysis, we will focus on labeled neurons outside the injection site.

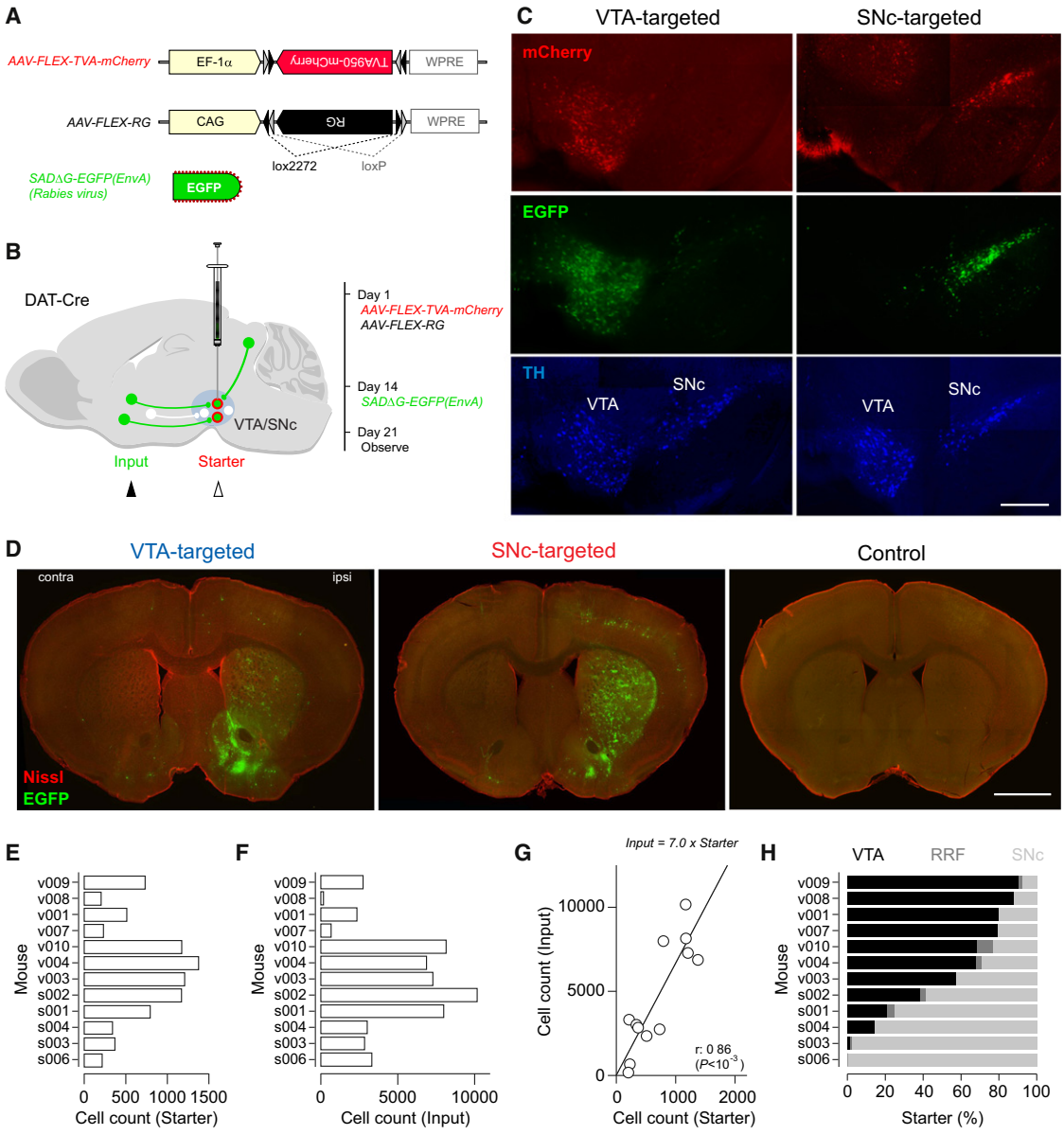

Figure 1. Identification of Monosynaptic Inputs to Midbrain Dopamine Neurons Using the Rabies Virus and Cre-Transgenic Mice

(A) Recombinant AAV strains and rabies virus.

(B) Experimental design.

(C) Characterization of the injection site at the ventral midbrain. Scale bar, 0.5 mm.

(D) Transsynaptically labeled neurons at the forebrain areas. The location of the coronal sections is indicated by the black arrowhead in (B). Left, v004; Middle, s002; Right, control with wild-type mouse. Scale bar, 1 mm. In all images, the right side corresponds to the side ipsilateral to the injected side.

(E) Numbers of starter neurons.

(F) Numbers of transsynaptically labeled neurons ("input neurons").

(G) Relationship between numbers of starter and input neurons.

(H) Proportions of labeled neurons in each of the midbrain dopamine nuclei. RRF, retrorubural field (A8).

Distinct Areas Project to Dopamine Neurons in VTA and SNc

Figure 2 shows the sections obtained from two mice that were administered the selective injections into VTA and SNc (v001 and s003; see Figure 1H). Using custom software, we identified anatomical areas based on a standard mouse atlas (Franklin and Paxinos, 2008) using fluorescent Nissl staining; the location of each neuron was registered on the anatomical coordinate. We then counted the number of neurons in each area. To correct for the variability in the total number of neurons, the numbers

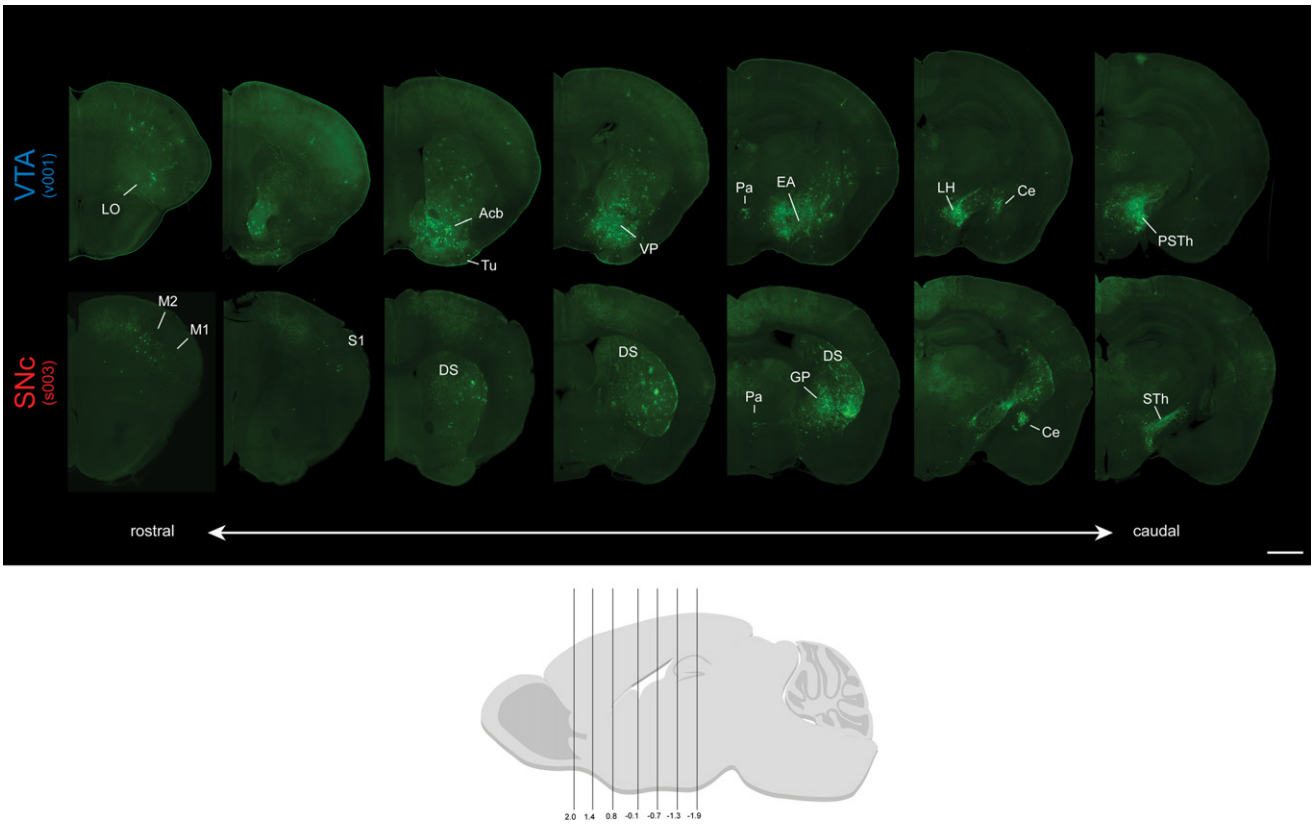

Figure 2. Distinct Areas Project to VTA and SNc Dopamine Neurons

Series of coronal sections for VTA- and SNc-targeted cases (v001 and s003, respectively). Only the side ipsilateral to the injection site is shown. Scale bar, 1 mm. LO, lateral orbital cortex; M1, primary motor cortex; M2, secondary motor cortex; S1, primary somatosensory cortex; Acb, nucleus accumbens; Tu, olfactory tubercle; DS, dorsal striatum; VP, ventral pallidum; Pa, paraventricular hypothalamic nucleus; EA, extended amygdala; GP, globus pallidus; LH, lateral hypothalamus; Ce, central nucleus of the amygdala; PSTh, parasubthalamic nucleus; STh, subthalamic nucleus.

were normalized by the total number of input neurons (Figure 3, left; Figure S2). We further computed the density of labeled neurons in each area by dividing the number by the area (mm^2) on each section (Figure 3, right). For each group, four animals that had preferential injections into VTA or SNc were used to generate Figure 3 (v009, v001, v010, and v004 for VTA; and s001, s004, s003, and s006 for SNc; note that v008 and v007 were not included because these mice had a small number of labeled neurons). Consistent results were obtained even when we restricted our analysis to three animals with higher specificity for each group. Furthermore, we have verified that the patterns of labeling are similar at 5 days (n = 3 mice, VTA) and 9 days (n = 2 mice, VTA) after the injection of SADΔG-GFP(EnvA) compared to the main data set obtained at 7 days after injection (Pearson correlations for the mean numbers of labeled neurons across areas were $r = 0.82$ and 0.95 between 5 versus 7 days and 7 versus 9 days, respectively; $p < 10^{-7}$ for both). This suggests that the results we report here are temporally stable and not affected by gross cell death over time.

Basal Ganglia and Hypothalamus: Global Shift of Input Areas

Across the whole brain, the most abundant labeling was found in the basal ganglia (striatum and pallidum) (Figure 3). In these areas, labeled neurons are predominantly found ipsilateral to the injection site (e.g., Figure 1D). Both for VTA- and SNc-targeted animals, labeled neurons formed continuous bands that ran from the striatum to specific hypothalamic areas (Figure 2). The densely labeled bands for VTA and SNc dopamine neurons showed rough segregation such that the areas projecting to SNc dopamine neurons were found in the more dorsal and lateral parts in this continuum, relative to those projecting to VTA dopamine neurons (Figures 2–4). These bands often did not reflect the boundaries of anatomically identified areas (Franklin and Paxinos, 2008), but the densely labeled regions included various areas in the striatum and pallidum and, more posteriorly, the basal forebrain and hypothalamus (Figures 2–4). In terms of numbers, the most prominent labeling was observed in the striatum partly due to its large volume, with greater emphasis on the ventral portion (nucleus accumbens [Acb] and olfactory tubercle [Tu]) in VTA-targeted mice and on the DS in SNc-targeted mice. In the amygdala, the central nucleus of the amygdala (Ce; in particular, the lateral central nucleus of amygdala [CeL]) was found to project to both VTA and SNc dopamine neurons (e.g., Figures 4D and 4E) while other amygdala regions, including the cortical amygdala, did not project much to dopamine neurons in either area.

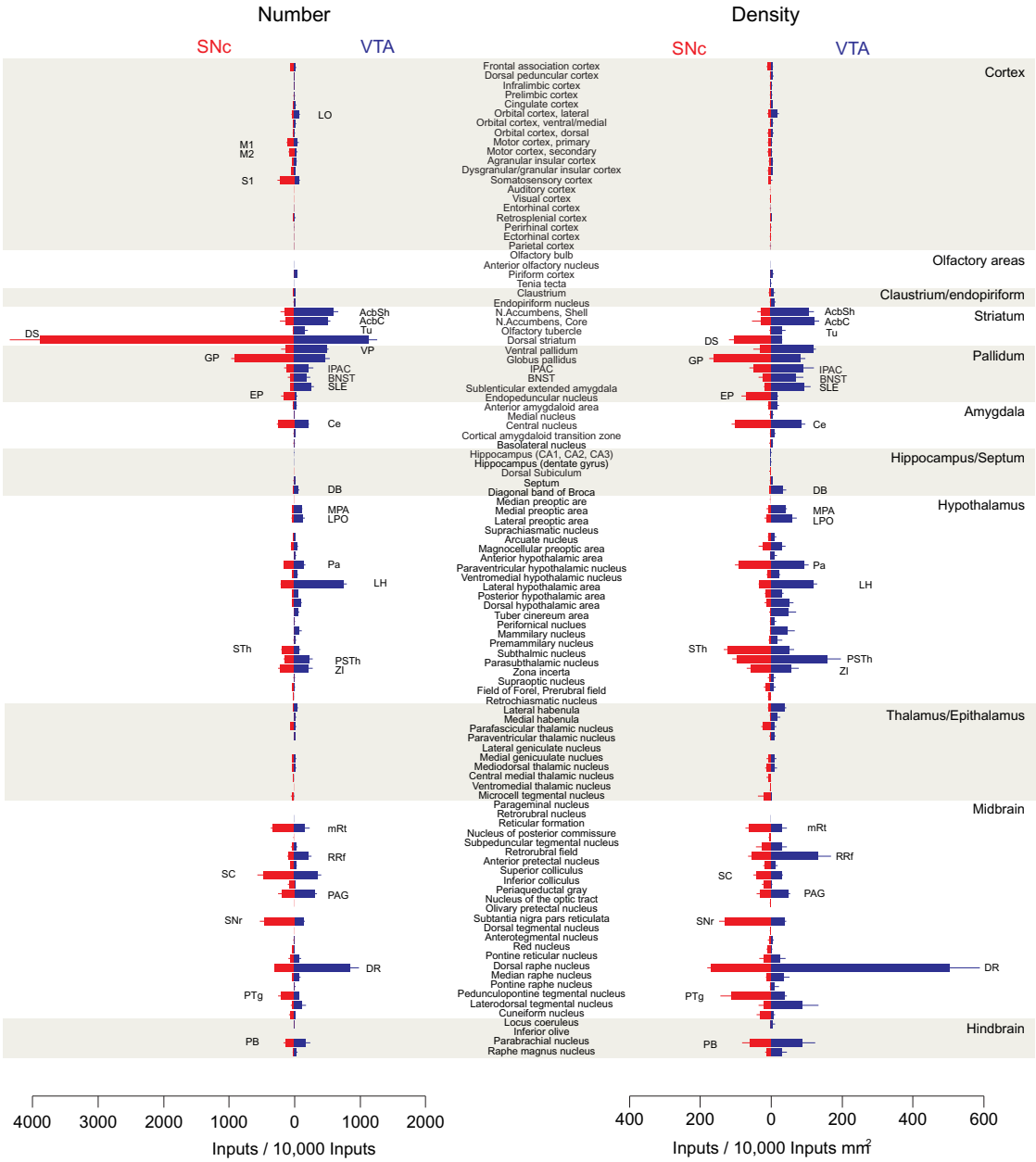

Figure 3. Comparison of Input Areas between VTA and SNc Dopamine Neurons

(Left) Number of input neurons in each area. Numbers are normalized by the total number of input neurons. Mean ± SEM (n = 4 mice).

(Right) Density of input neurons in each area. Mean ± SEM. BNST, bed nucleus of stria terminalis; IPAC, interstitial nucleus of the posterior limb of the anterior commissure; Extended amygdala and substantia innominata are included in sublenticular extended amygdala (SLE).

In pallidal areas, more ventral and medial structures such as the ventral pallidum (VP) and sublenticular extended amygdala (EA) project predominantly to VTA dopamine neurons, whereas more dorsal and lateral structures such as the globus pallidus (GP) and entopeduncular nucleus (EP) project predominantly to SNc dopamine neurons (Figures 4A–4C). The bed nucleus of stria terminalis (BNST; in particular, its dorsal lateral division [STLD]) projects to both VTA and SNc (Figure S6A).

From the basal forebrain and hypothalamic areas, VTA dopamine neurons receive the greatest input from the LH (including the peduncular part of the lateral hypothalamus [PLH]). VTA dopamine neurons also receive inputs from scattered neurons in the diagonal band of Broca (DB) and medial and lateral preoptic areas (MPA and LPO) (Figures 3, 4A, 4D, and S3C). In these areas, the paraventricular hypothalamic nucleus (Pa) is unique in that it contains densely labeled neurons, for both VTA- and SNc-targeted cases (Figure S6B). In contrast, in SNc-targeted cases,

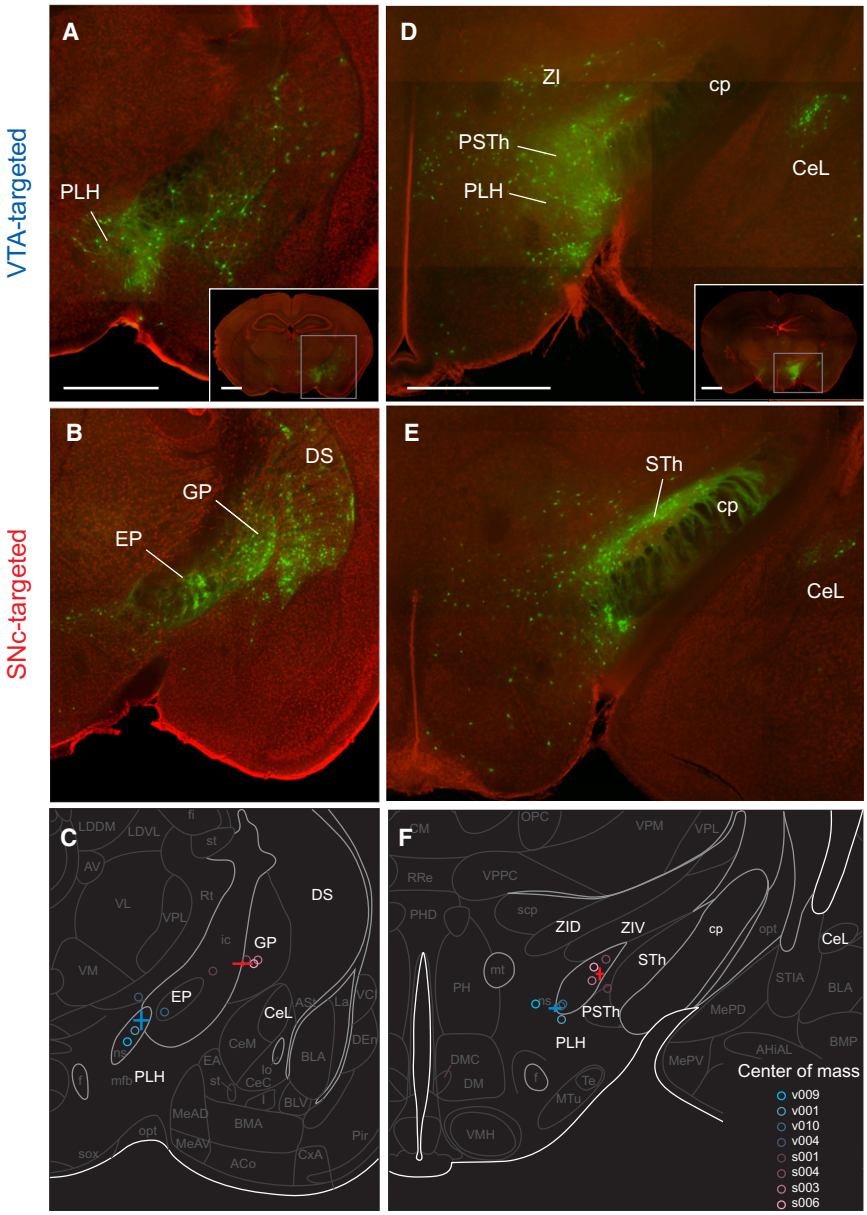

Figure 4. Input Areas for VTA and SNc Dopamine Neurons Are Spatially Shifted in the Basal Ganglia and Hypothalamus

(A–C) Striatal and pallidal area. (A) VTA-targeted. (B) SNc-targeted. Green, EGFP; Red, fluorescent Nissl staining. (C) The center of mass of input neurons. Circles indicate the centers of mass from individual animals. The blue and red crosses indicate the mean ± SEM across animals (n = 4 mice for each group). PLH, peduncular part of the LH; DS, dorsal striatum; GP, globus pallidus; EP, entopeduncular nucleus. Right, lateral. Scale bar, 1 mm.

(D–F) Hypothalamic areas. Same conventions as (A) through (C). PSTh, parasubthalmic nucleus; ZI: zona incerta; ZID, dorsal zona incerta; ZIV, ventral zona incerta; cp, cortical peduncle; CeL, lateral division of the central nucleus of the amygdala (Ce); STh, subthalamic nucleus.

fewer neurons were labeled in hypothalamic areas except Pa, while the STh contained a dense collection of neurons that project preferentially to SNc dopamine neurons (Figures 4D–4F). Para-STh (PSTh) and zona incerta project both to VTA and SNc dopamine neurons with a slight bias to VTA. Together, these results show that VTA and SNc dopamine neurons receive input from largely segregated, continuous "bands" in the basal ganglia and hypothalamus. Interestingly, LH and STh provide contrasting preferential inputs to VTA and SNc, respectively.

Cortical Projections: Direct Inputs from Rostral Neocortex

We found significant monosynaptic input from cortical areas (Figures 3 and 5). In the neocortex, labeled neurons are widely distributed across cortical areas (Figures 5A–5F). To visualize the distributions of labeled neurons across entire cortical areas, we generated "unrolled maps" of the neocortex. For each section, we projected labeled cortical neurons on to a line running through the middle of the cortical sheet (Figures 5C, 5F–5H). The same method was applied to a standard atlas to generate a reference map (Figure 5I). This analysis revealed that labeled neurons are localized mostly in the rostral half of the cortical sheet encompassing motor, somatosensory, medial prefrontal, and orbitofrontal areas. In contrast, very sparse labeling was found in the caudal half, the parietal, visual, auditory, and entorhinal cortices. In SNc-targeted cases, the most dense labeling was found in the primary and secondary motor cortices (M1 and M2) (Figures 5B, 5E, 5H, and S4). Somatosensory cortex (S1) has moderate labeling, but, due to its large size, it provides the largest number of inputs among cortical areas (Figure 3). VTA dopamine neurons receive fewer cortical inputs than SNc dopamine neurons, but the lateral orbitofrontal cortex (LO) is the major sources of cortical inputs to VTA dopamine neurons (Figures 3, 5A, and 5G). Areas encompassing the medial prefrontal cortex (PrL, IL, DP, and MO) and the cingulate cortex (Cg1 and Cg2) have moderate labeling. These results demonstrate that dopamine neurons in the VTA and SNc receive significant numbers of cortical inputs from overlapping but distinct areas.

Midbrain and Hindbrain: Discrete Foci

At more caudal regions, the intermediate layer of the superior colliculus (SC) and supraoculomotor (ventrolateral) periaqueductal gray (PAG) contained large numbers of labeled neurons in both VTA- and SNc-targeted cases (Figure S6C). The dorsal raphe (DR) contained the densest population of labeled neurons both for VTA- and SNc-targeted cases, with slightly stronger

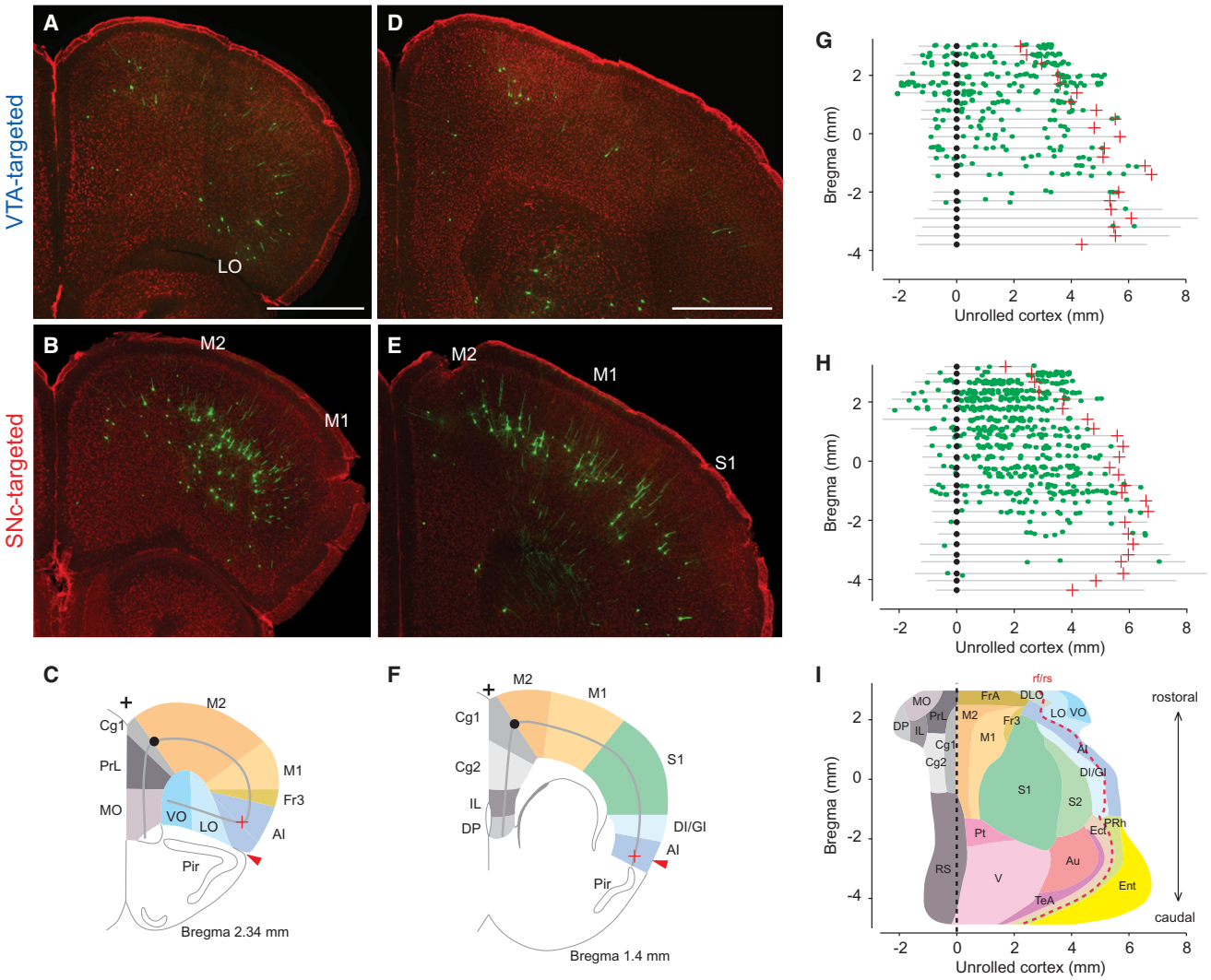

Figure 5. Widespread Cortical Neurons Project Directly to VTA and SNc Dopamine Neurons

(A and B) Distributions of input neurons for (A) VTA- and (B) SNc dopamine neurons. LO, lateral orbital cortex; M1, primary motor cortex; M2, secondary motor cortex. Scale bar, 1 mm.

(C) Schematic of cortical areas at the similar bregma level (2.34 mm) as defined by Franklin and Paxinos (2008). Unrolled maps in (G) and (H) were generated by projecting labeled neurons on to the gray line that runs through the middle of the cortical sheet. Two reference points on the gray line (black dot and red cross) were defined by projecting the most dorsomedial point on the hemisphere (black cross) and the rhinal fissure (red arrowhead).

(D–F) Another example from a more posterior section (Bregma: + 1.4 mm). S1, primary somatosensory cortex. Scale bar, 1 mm.

(G) Unrolled map of input neurons obtained in one VTA-targeted animal (v004, same as in A and D). Each green dot represents a single EGFP-labeled neuron.

(H) Unrolled map of input neurons obtained in one SNc-targeted animal (s001, same as in B and E).

(I) Unrolled representation of cortical areas as defined in a standard mouse atlas (Franklin and Paxinos, 2008). AI, agranular insular cortex; AIP, agranular insular cortex, posterior part; Au, auditory cortex; Cg1, cingulate cortex area 1; Cg2, cingulate cortex area 2; DI, dysgranular insular cortex; DLO, dorsolateral orbital cortex; DP, dorsal peduncular cortex; Ect, ectorhinal cortex; Ent, entorhinal cortex; FrA, frontal association cortex; Fr3, frontal cortex area 3; GI, granular insular cortex; IL, infralimbic cortex; MO, medial orbital cortex; PRh, perirhinal cortex; PrL, prelimbic cortex; Pt, parietal cortex; RS, retrosplenial cortex; S2, secondary somatosensory cortex; TeA, temporal association cortex; V, visual cortex; VO, ventral orbital cortex.

projections to VTA (Figure S6D; also see Figure 3). The pedunculotegmental nucleus (PTg) and cuneiform nucleus (CnF) preferentially project to SNc dopamine neurons, whereas laterodorsal tegmental nucleus (LDTg) preferentially projects to VTA dopamine neurons (Figure S6D). The parabrachial nucleus (PB), both ipsilateral and contralateral to the injection side, projects to both VTA and SNc dopamine neurons (Figure S6E). We also found that cerebellar nuclei project to dopamine neurons (Figure S6F).

The aforementioned results are, to a large degree, consistent with previous results using conventional tracers (Geisler and Zahm, 2005) but differ in some critical ways. For example, some areas such as the septum and mHb were not labeled heavily in our experiment, despite being strongly labeled in

previous experiments involving injection of a retrograde tracer (Fluoro-gold) in VTA (Geisler and Zahm, 2005). Furthermore, even in the areas that were labeled both in our and in other previous experiments, our methods resulted in labeling of more specific subsets of neurons (see below). To test whether these differences are due to the greater specificity of our labeling methods, we performed a control experiment using rabies virus that was not pseudotyped with EnvA but still lacks RG (SADΔG-GFP) (therefore, this virus can infect mammalian cells but cannot spread transsynaptically). In these experiments, injection of the virus into VTA resulted in a significant number of retrogradely labeled neurons in the septum and mHb (Figures S3A, S3B, S3D, and S3E). Furthermore, in the hypothalamus, labeled neurons were scattered widely with the nonpseudotyped virus, although the pseudotyped virus labeled more confined populations, resulting in densely labeled Pa and LH surrounded by largely negative areas (Figures S3C and S3F). This implies that previous results may be explained by inputs to nondopaminergic neurons in (or near) the VTA and SNc.

In short, we demonstrate various connections that have been largely overlooked in previous studies (e.g., M1, M2, S1, and STh). Furthermore, these results allowed for comprehensive and direct comparisons of the inputs to VTA and SNc dopamine neurons.

Specific Populations of Striatal Neurons Project to Dopaminergic and GABAergic Neurons in SN

The aforementioned observation that a large number of striatal neurons project directly to dopamine neurons appears to contradict recent optogenetic studies indicating that striatal neurons form synapses almost exclusively on to nondopaminergic neurons (presumed GABAergic neurons) in VTA or SN (Chuhma et al., 2011; Xia et al., 2011). To address this issue, we performed transsynaptic tracing from GABAergic neurons in the SN using transgenic mice that express Cre in GABAergic neurons (vesicular GABA transporter-Cre or Vgat-ires-Cre) (Vong et al., 2011).

The DS is divided into subregions, so-called patch and matrix compartments, that can be defined by the expression of molecular markers such as calbindin D-28k (Gerfen, 1992; Graybiel, 1990). Previous studies have suggested that the medium spiny neurons in the patch compartments project to SNc while those in the matrix project to SNr (Fujiyama et al., 2011; Gerfen, 1984), although this idea was later cast into doubt (Lévesque and Parent, 2005). More importantly, cell-type specificity of target neurons has not been demonstrated. We therefore sought to test the hypothesis that the patch and matrix separately project to dopaminergic and GABAergic neurons, respectively. We reasoned that, given the close proximity of dopaminergic and GABAergic neurons in SN, such separation would support the specificity of our transsynaptic tracing.

A closer look at the distribution of labeled neurons in the striatum showed that neurons labeled in DAT-Cre mice tended to form clusters (Figure 6A). These clusters were found in areas that correspond to the patches (including the "subcallosal streak"), defined by low calbindin D-28k levels (Figures 6B and 6C), although the boundary of patches and matrices is not always clear and some labeled neurons were observed outside of the boundary. In contrast, neurons labeled in Vgat-ires-Cre mice showed little clustering and were found in the matrix defined by higher calbindin D-28k levels (Figures 6E–6G). Quantification of fluorescent levels in cell bodies showed that most of the neurons projecting to dopamine neurons expressed calbindin D-28k to a much lower degree, compared to neurons projecting to GABAergic neurons (Figure 6I).

Furthermore, we found that labeled neurons in the two conditions showed different morphologies (Figures 6D, 6H, 6J, and 6K). In neurons projecting to GABAergic neurons, dendrites spread radially outward. In contrast, in neurons projecting to dopamine neurons, dendrites curved and coursed circuitously or turned inward toward the soma (Figure 6K). Furthermore, spines of inputs to GABAergic neurons were evenly spaced and were of similar size. In contrast, inputs to dopamine neurons had uneven spines and varicosities, and their dendrites were irregular in contour (Figures 6D and 6H, inset). These results suggest that, whereas neurons projecting to GABAergic neurons are consistent with typical medium spiny neurons, neurons projecting to dopaminergic neurons have significantly different morphologies. We make two conclusions from these data: First, striatal neurons do project monosynaptically to dopamine neurons; and second, our technique is capable of revealing exquisite, cell-type-specific connectivity.

Dopamine-Projecting Neurons in the Acb Form Patches

Whereas SNc dopamine neurons receive the most input from the DS, VTA dopamine neurons receive the most input from the Acb (Figure 3). Although heterogeneity of the Acb was reported previously with different molecular markers (Zahm and Brog, 1992), a patch/matrix organization has not been documented consistently. We found that neurons that project to dopamine neurons form patches in the VS, albeit much larger than the patches found in the DS (Figure 7). These "ventral patches" contain extremely dense groups of labeled neurons (Figure 7A). Staining of calbindin D-28k showed that EGFP-positive neurons were found preferentially where calbindin D-28k expressions are lower, although dopamine-neuron-projecting patches were smaller than areas defined by weak staining of calbindin D-28k (Figures 7B–7D). Comparison across animals indicates stereotypical patterns of dopamine neuron-projecting patches (Figures 7E–7J; Figure S5). For this, we first identified regions with high density of labeled neurons ("predicted patches") using four of five animals tested (v009, v001, v010, v004, and v003). In the one remaining animal, we then obtained the proportion of labeled neurons that fell into the contour of the predicted patches. This proportion was then compared against that expected from a random distribution (i.e., percentage of the Acb contained within the predicted contours). This analysis showed that neurons tended to localize within the contours obtained from other animals (Figure 7J; $p < 0.02$, paired t test). These results support the idea that Acb neurons indeed project to dopamine neurons and that most of these neurons are clustered in stereotypical locations, or "ventral patches," which were overlooked in previous studies.

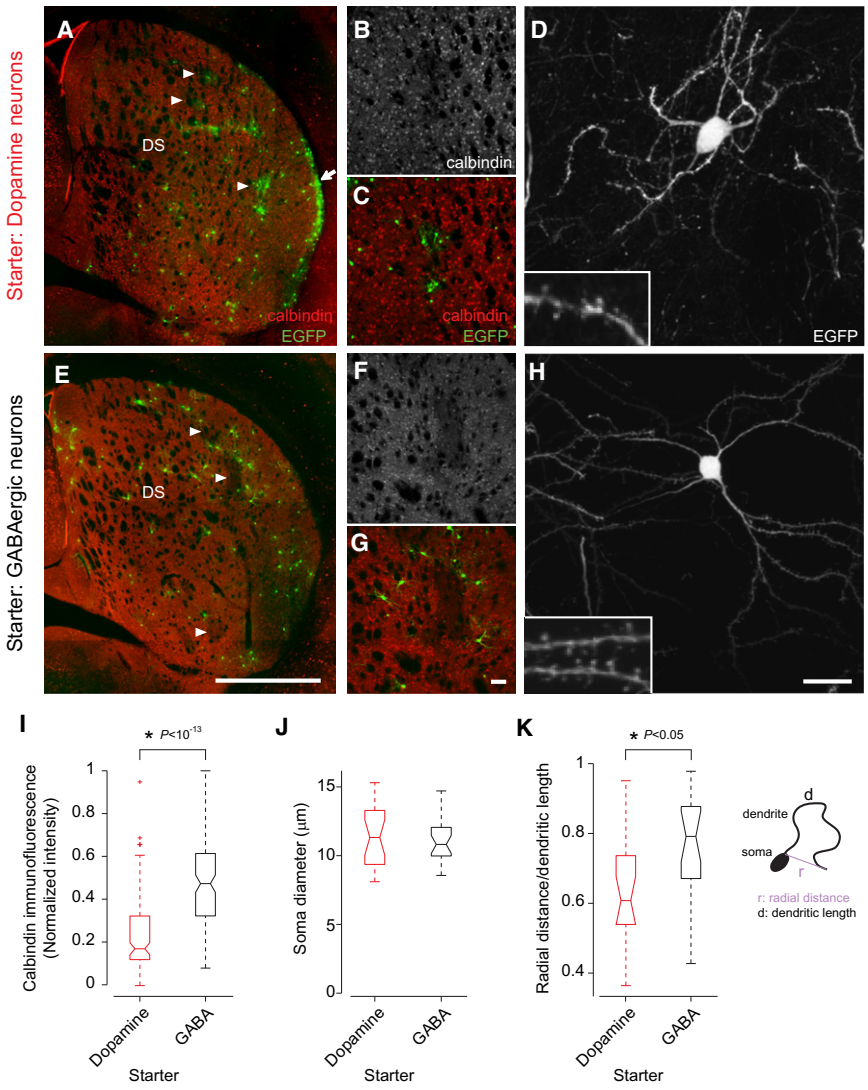

Figure 6. Dopamine and GABA neurons in SN Receive Inputs from Striatal Neurons in Patch and Matrix, Respectively

(A) Distribution of neurons projecting to SNc dopamine neurons. A low-magnification view of the dorsal striatum (DS) in a DAT-Cre mouse. Red, calbindin D-28k immunostaining. Green, EGFP (input neurons). Subcallosal streak is indicated by an arrow. Representative patches are indicated by arrowheads.

(B) Higher magnification view stained for calbindin D-28k.

(C) Higher magnification view showing the locations of input neurons with respect to calbindin D-28k staining.

(D) Morphology of a labeled neuron. The inset shows a high-magnification view of a dendrite.

(E–H) Distribution and morphology of neurons projecting to SN GABAergic neurons. The results were obtained using Vgat-ires-Cre mice. Scale bars, 1 mm in (E), 80 μm in (G), and 20 μm in (H).

(I) Quantification of calbindin D-28k expression levels. $p < 10^{-13}$, t test (n = 126, 68 neurons). In box plots, the central mark represents the median, and the edges of the box are the 25th and 75th percentiles.

(J) Quantification of the cell body size (diameter). $p > 0.05$, t test (n = 23, 25 neurons).

(K) Quantification of the complexity of the dendrites. r, radial distance (straight line distance between the cell body and the tip of dendrites); d, dendritic length. $p < 0.03$, t test (n = 20, 20 neurons).

DISCUSSION

In the present study, we developed a technique to obtain a comprehensive list of monosynaptic inputs to midbrain dopamine neurons. Our direct comparison of inputs to VTA and SNc dopamine neurons resolves several outstanding questions that previous methodologies lacked the specificity to address. We demonstrate that SNc dopamine neurons receive direct input from the somatosensory and motor cortices and from the STh. In contrast, VTA dopamine neurons receive input from the LH and, to a lesser extent, the LO. Furthermore, we show that the DS and VS project directly to SNc and VTA dopamine neurons, respectively, thus resolving a recent dispute over whether neurons in the striatum project directly to dopamine neurons, as was long assumed. The results also reveal that striatal neurons that project to dopamine neurons form patches both in the DS and VS. These results thus provide foundational knowledge on the different inputs to VTA and SNc dopamine neurons as well as the basic organization of the basal ganglia circuit.

High Specificity of Transsynaptic Tracing by Cre-Transgenics with Rabies Virus

Rabies-virus-based transneuronal tracing is expected to play an important role in elucidating neuronal connectivity (Callaway, 2008; Ugolini, 2011). Interpretation of the results, however, critically depends on the specificity and generality of the tracing (that is whether rabies can propagate to all synaptically connected neurons). We successfully labeled diverse cortical and subcortical areas that appear to differ in their neurotransmitter types, modes of firing, and functions. Although most of our findings matched conventional tracing experiments, there were several important exceptions, in which we failed to observe labeling in regions previously thought to project to VTA and/or SNc. Most of these areas (septum, mHb, striatal neurons in the matrix compartment) were labeled by nonspecific rabies virus or were from GABAergic neurons, indicating that these structures project to nondopaminergic neurons in VTA and/or SNc or that their axons pass through these areas. Most importantly, we were able to label largely separate neuronal populations in the striatum, those in patch and matrix compartments, which project to dopaminergic and GABAergic neurons respectively, in the SN. Given that dendrites of SNc dopaminergic neurons extend to the SNr where GABAergic neurons reside, the result

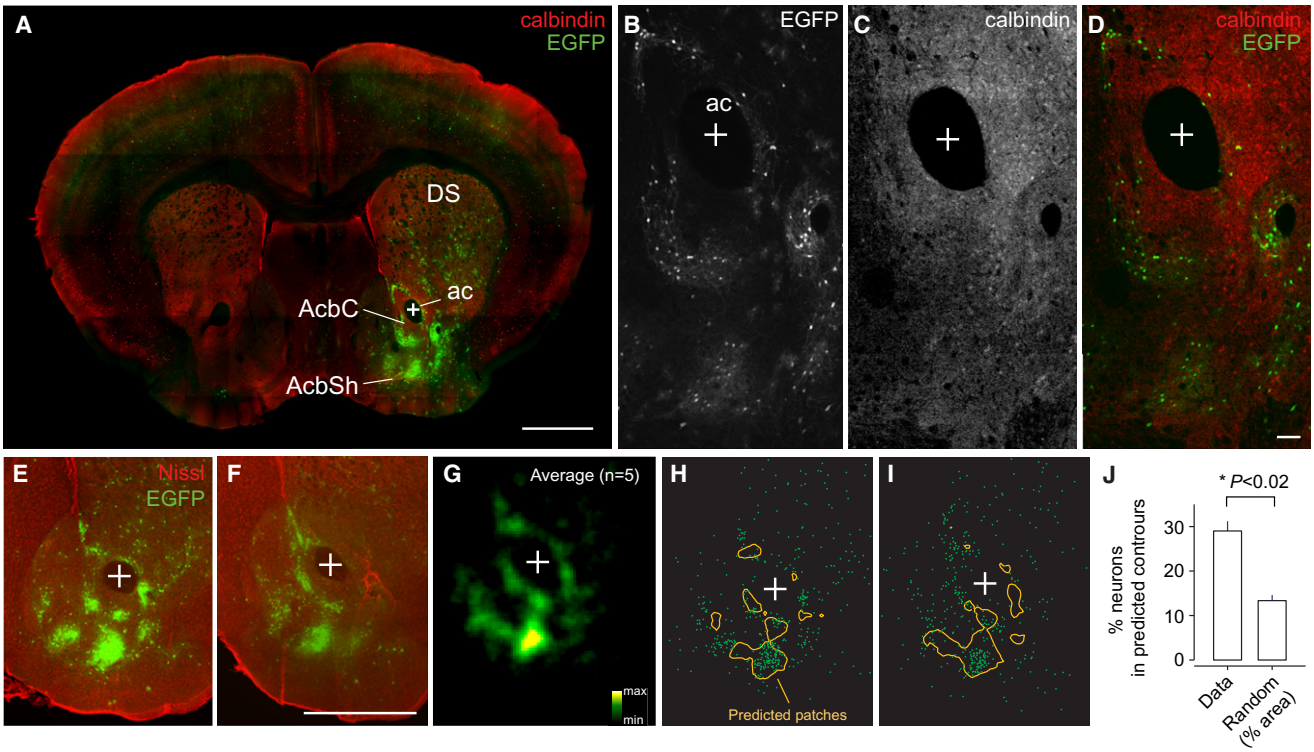

Figure 7. Dopamine-Projecting Neurons in the Acb Form Patches

(A) Coronal section containing the Acb of a VTA-targeted animal (v003). Red, calbindin D-28k immunostaining; green, EGFP (input neurons); ac, anterior commissure; AcbC, nucleus accumbens core; AcbSh, nucleus accumbens shell; DS, dorsal striatum. Plus sign indicates the center of the ac. Scale bar, 1 mm.

(B–D) Medium magnification views of the Acb in (A). The same section as in (A), but the images were obtained using a confocal microscope resulting in a thin optical section. Scale bar, 80 μm.

(E and F) Example distributions of input neurons in two animals. In (E), v010; in (F), v004. Scale bar, 1 mm.

(G) Average density map obtained using the five VTA-targeted animals (v009, v001, v010, v004, and v003).

(H and I) "Predicted patches" (orange contours) superimposed on the distribution of input neurons in two animals (same as in E and F). The contours of predicted patches were obtained using data from the four other animals, not the animal's own data.

(J) Percentage of neurons located in the predicted patches ("Data") compared to the percentage of the Acb taken up by patches ("Random"). The latter represents the percentage expected when neurons are randomly distributed. Mean ± SEM, $p < 0.02$, paired t test (n = 5 mice).

suggests that transneuronal spread does not occur through mere proximity.

One caveat of the present method (common to other retrograde tracing methods) is that a small amount of labeling does not necessarily indicate functionally weak connectivity. For example, one input neuron may form synapses on to many postsynaptic neurons, and a small number of synapses may nonetheless be strong. Therefore, some of the discrepancies between the present and previous studies may be, at least in part, explained by these limitations. These issues need to be addressed using anterograde tracing or electrophysiological examinations. Nevertheless, although future experiments need to validate the method further, our results together with existing literature (Callaway, 2008; Ugolini, 2011) support the utility of rabies virus-mediated transsynaptic tracing.

Our methods have further technical advantages over conventional methods. First, the ability to target the tracer (initial infection of the virus) was greatly aided by the use of Cre-transgenic mice. This is in contrast with conventional tracing experiments in which the accuracy of targeting largely depends on the precise positioning of the injection pipet and proper injection parameters. A similar approach was first introduced using pseudorabies (DeFalco et al., 2001; Yoon et al., 2005), but the transsynaptic spread was not restricted to monosynaptic inputs. Second, our ability to directly identify starter neurons by fluorescent markers is useful for quantitative analyses. With conventional methods, it is often difficult to distinguish between direct depositions and transported tracers. Our use of a fusion protein between a transmembrane type of TVA (TVA950) and mCherry allowed us to directly identify starter neurons and appears to be a viable approach. Third, the high efficiency of the tracing enables comprehensive mapping that consistently covers most areas in each animal. Fourth, extremely high expressions of fluorescent markers with rabies virus allowed for observations of detailed morphologies of individual neurons (Wickersham et al., 2007a). Due to the strong signal, low magnification images obtained using semiautomatic acquisitions were sufficient for identifying labeled neurons. These characteristics are useful for systematic and quantitative mapping of neuronal connectivity and will facilitate future high-throughput efforts.

Distinct Inputs to SNc and VTA May Explain Their Saliency- and Value-Related Activity

Our data show that VTA and SNc dopamine neurons receive distinct excitatory inputs. This may help explain recent electrophysiological data from nonhuman primates. Matsumoto and Hikosaka (2009) found that, whereas VTA dopamine neurons are excited and inhibited by appetitive and aversive events, respectively, dopamine neurons in the lateral SNc are excited by both. Furthermore, response latencies were generally shorter in dopamine neurons in the lateral SNc. Our data suggest that distinct excitatory inputs to VTA and SNc dopamine neurons may provide value- and saliency-related information differently to these neurons. Note, however, that there are important anatomical differences between dopamine neurons in rodents and primates (Berger et al., 1991; Joel and Weiner, 2000). For example, dopamine neurons that project to the NAc are contained not only in VTA but also the medial part of SNc in primates, whereas they are more confined to VTA in rodents, suggesting that the position of the VTA/SNc boundary might be shifted between primates and rodents (Brog et al., 1993; Joel and Weiner, 2000; Lynd-Balta and Haber, 1994). Therefore, comparisons between species need to be done carefully.

Previous studies proposed that inputs from the Ce, PB, SC, and the basal forebrain may account for short-latency activations of SNc dopamine neurons (Bromberg-Martin et al., 2010; Coizet et al., 2010; Dommett et al., 2005; Matsumoto and Hikosaka, 2009). Contrary to these proposals, however, our data showed that the Ce, PB, and SC project strongly to both VTA and SNc dopamine neurons (although SC has a slight preference for the SNc). The basal forebrain (originating mainly from the DB) was found to project preferentially to VTA dopamine neurons.

Instead, our data showed that there are specific projections from S1 and motor cortices (M1 and M2) to SNc dopamine neurons. Whether the neocortex directly projects to the SNc, and where in the cortex these inputs originate, have received less attention partly due to inconsistent results in previous studies (Bunney and Aghajanian, 1976; Graybiel and Ragsdale, 1979; Naito and Kita, 1994; Zahm et al., 2011). Although the role of somatosensory and motor inputs in dopamine regulation has not been fully explored previously, somatosensation constitutes an important component of rewarding and noxious stimuli. Furthermore, dopamine neurons increase their firing when an animal initiates reward-oriented behavior (Jin and Costa, 2010). Given that these cortical inputs are most likely excitatory, they may play a role in short-latency activation of SNc dopamine neurons in response to stimuli predicting salient events or the salient stimulus itself.

We also found that the STh provides specific and relatively strong inputs to SNc dopamine neurons. Previous studies found only sparse projections from the STh to the SNc using anterograde tracers (Groenewegen and Berendse, 1990; Kita and Kitai, 1987; Smith et al., 1990). One possible reason for this discrepancy is that dopamine neurons receive STh inputs at their dendrites that elongate into SNr. STh neurons respond to various motor events and rewards as well as a sudden change in the environment (Isoda and Hikosaka, 2008; Matsumura et al., 1992). Anatomically, STh constitutes the "hyperdirect pathway" as well as the "indirect" pathway of the corticobasal ganglia loops (Nambu et al., 2002) (Figure 8C). The former term emphasizes the high conduction velocity of this pathway. On the other hand, the LH is a major input for VTA dopamine neurons. LH neurons are known to process reward information (Ono et al., 1986), and these responses are modulated by internal states of the animal such as hunger (Burton et al., 1976), indicating that LH responses reflect subjective values. Our results together with previous findings raise the possibility that STh and LH provide contrasting excitatory inputs encoding saliency- and value-related information, respectively.

Direct Projections from the Striatum to Dopamine Neurons: Patch/Matrix Projection Systems and Computation of Reward Prediction Errors

The striatum has received much attention as an important input to dopamine neurons. For example, various computational models of reinforcement learning posit an important role for direct projections of striatal neurons to dopamine neurons in calculating reward prediction error (Doya, 1999; Houk et al., 1996; Joel et al., 2002; Suri, 2002). Recent studies have indicated, however, that direct projections from striatal neurons to dopamine neurons are weak or nonexistent (Chuhma et al., 2011; Xia et al., 2011). Contrary to these recent results, our study demonstrates that, in terms of numbers, the striatum is the most prominent input to both VTA and SNc dopamine neurons. Although we cannot rule out the possibility that the striatum-dopamine neuron synapses are mostly "silent," the prominent labeling and exquisite specificity indicate that this connection exists. Our result indicates that only a very specific, small subset of striatal neurons project to dopamine neurons. This raises the question as to whether channelrhodopsin was expressed in this particular population in the previous experiments. Another possible explanation is that these synapses use a different neurotransmitter than GABA.

Our results have implications for the basic organizing principle of the basal ganglia circuit. Corticobasal ganglia circuits form multiple, parallel pathways between the cortex and the output structures of the basal ganglia (i.e., EP and SNr) (Figure 8). The DS can be parceled into patch and matrix compartments that may define distinct projection systems (Gerfen, 1992; Graybiel, 1990). Previous studies have indicated that striatal neurons in the patches project to SNc, whereas those in the matrix project to SNr (Fujiyama et al., 2011; Gerfen, 1984), although a recent study indicated that these projections are not as specific as previously thought, at least in primates (Lévesque and Parent, 2005), and the cell-type specificity of postsynaptic neurons has not been established. We extend the previous findings by showing that the patch-matrix system represents segregated neural pathways that comprises distinct types of neurons both pre- and postsynaptically (Figure 8C). Importantly, dopamine-neuron-projecting striatal neurons differ from GABAergic-neuron-projecting medium spiny neurons in their morphology and calbindin D-28k expression, suggesting that these neurons are a new class of medium spiny neurons. Furthermore, we showed that the Acb also has dopamine-neuron-projecting patch structures, which are smaller than the shell/core divisions defined by molecular markers (Figure S5). A recent study found

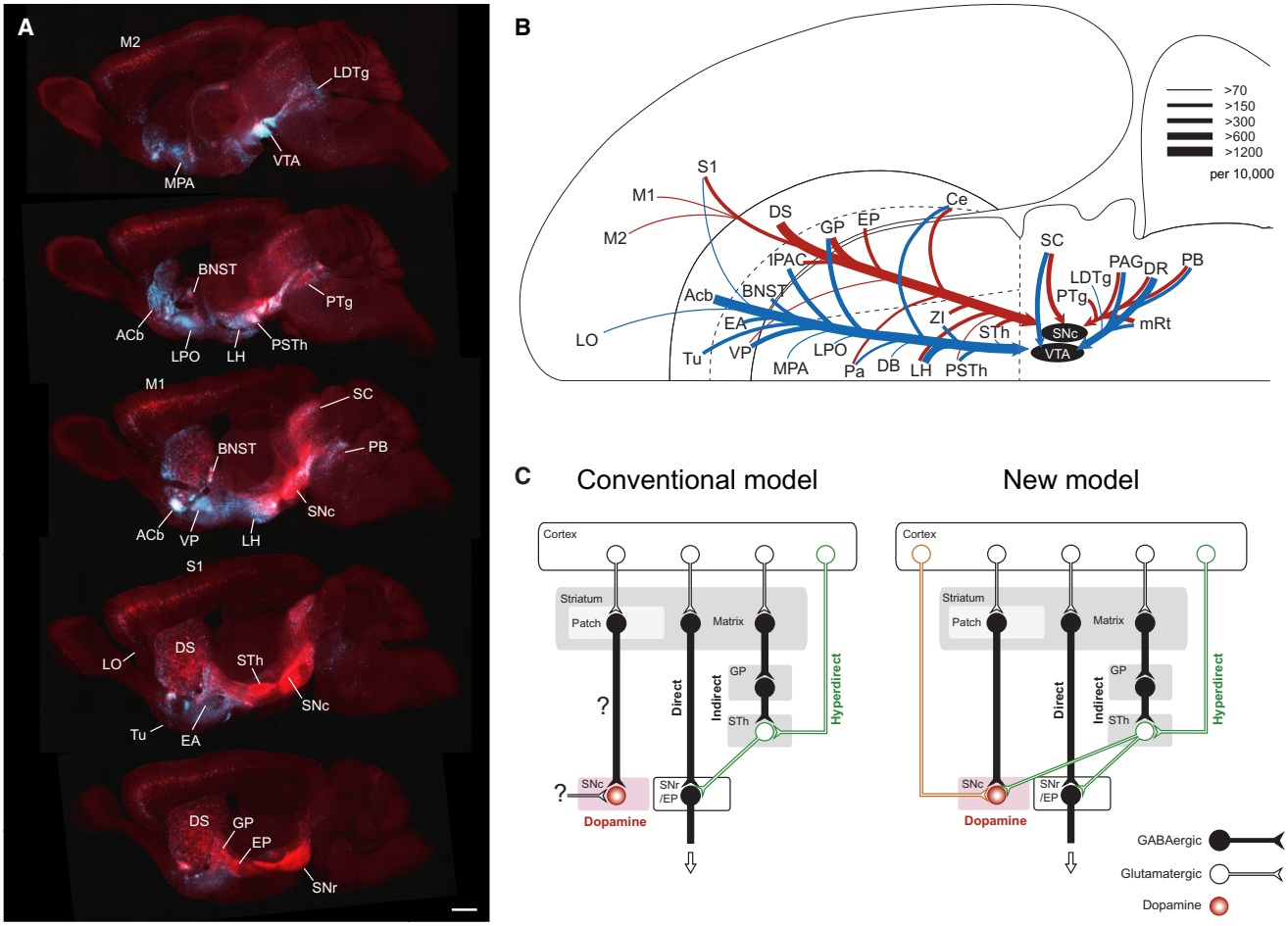

Figure 8. Summary of the Connectivity

(A) Direct comparison of the distributions of monosynaptic inputs to VTA and SNc dopamine neurons. SADΔG-EGFP(EnvA) and SADΔG-mCherry(EnvA) were injected into VTA and SNc, respectively. Cyan: VTA targeted. Red: SNc targeted. Top, medial. Bottom, lateral. Scale bar, 1 mm.

(B) Flatmap summary of monosynaptic inputs to VTA and SNc dopamine neurons. Blue indicates inputs to VTA. Red indicates inputs to SNc dopamine neurons. The thickness of each line indicates the number of input neurons in each area (inputs per 10,000 total inputs) as defined at the top right corner. The flatmap representation is after Swanson (2000). Connections from DS to VTA and Acb to SNc were omitted for clarity.

(C) Models of the corticalbasal ganglia circuit. Left, conventional model; right, new model based on the present result. Some connections are omitted for simplicity.

a "hedonic hotspot," a potential microdomain defined by the hedonic (or "liking") effect of opioids (Peciña and Berridge, 2005). Based on the available data, the hedonic hotspot (in rats) appears to lie just dorsal to one of the "ventral patches" we found (in mice). These results indicate that the VS also forms parallel channels for information flow.

Taken together, these results suggest that the corticobasal ganglia inputs to dopamine neurons form multiple pathways, akin to the corticobasal ganglia output pathways via EP and SNr: Dopamine neurons receive direct and indirect inputs from the striatum, inputs from the cortex via STh, and direct inputs from the cortex (Figure 8).

Inputs from Motor and Autonomic Areas

The comprehensive identification of inputs revealed that one common feature for both VTA and SNc is that many of the areas that project directly to dopamine neurons have been characterized as autonomic (Ce, lateral BNST, Pa, LH, PAG, and PB) (Saper, 2004). As mentioned earlier, SNc also receives inputs from motor areas (M1, M2, and STh). The central autonomic system receives taste and visceral information and regulates various autonomic responses (Saper, 2002; Yamamoto, 2006). Highly overlapping structures are also identified for pain processing (Gauriau and Bernard, 2002; Saper, 2002). Autonomic and motor responses are tightly coupled to rewarding as well as aversive events (and their expectations) or the saliency of sensory cues. In this sense, efferent copies of autonomic or motor signals may serve as a surrogate of important information for dopamine neurons, such as reward expectation and motivational saliency, in addition to general states of the animal. Although the role of these motor and autonomic inputs in the regulation of dopamine neuron activities is unclear, our finding

provides a framework with which to explore the mechanisms of dopamine neuron regulation.

Inputs from the PTg

It has been proposed that PTg plays an important role in reward prediction error computations (Kawato and Samejima, 2007; Okada et al., 2009). Previous studies have shown that electrical stimulation of PTg produced monosynaptic activation of dopamine neurons (Futami et al., 1995; Lokwan et al., 1999; Scarnati et al., 1984). Some anatomical studies have also indicated that PTg projects to both VTA and SNc using anterograde and retrograde tracing methods (Jackson and Crossman, 1983; Oakman et al., 1995; Zahm et al., 2011). These results appear to differ from our data indicating relatively sparse labeling of PTg from the VTA compared to SNc dopamine neurons. This difference may be explained if single PTg neurons make many synapses onto VTA dopamine neurons or synapses transmissions are strong. The aforementioned results may also be confounded by nonspecific electrical stimulation of passing fibers or uptake of tracers. Whether VTA receives strong direct inputs from PTg neurons remains to be clarified. Our method allowed us to avoid limitations of previous methods (i.e., cell-type specificity and labeling axons of passage), and the difference from other studies may come, at least in part, from the specificity achieved using our method although the exact reasons need to be clarified in the future. It should also be noted that other anatomical studies have indicated that VTA does not receive strong inputs from PTg (Geisler and Zahm, 2005; Phillipson, 1979).

Implications for Deep Brain Stimulation for Parkinson's Disease

Degeneration of SNc dopamine neurons leads to the severe motor impairments of Parkinson's disease. Symptoms of this disease can be ameliorated by high-frequency electrical stimulation of specific brain areas (deep brain stimulation [DBS]) (Benabid et al., 2009; Wichmann and Delong, 2006). Despite the wide use and success of DBS, its mechanisms remain highly debated, and it is unknown why specific targets are more effective than others.

The most popular target of DBS is the STh. As described earlier, we found relatively strong direct projections from the STh to SNc dopamine neurons. Interestingly, when the density of labeled neurons was calculated, the STh emerged as one of the highest density areas due to its small size. It is well known that symptoms improved by STh DBS coincide with those improved by levodopa (dopamine precursor) treatment, and patients' response to levodopa is the best outcome predictor of DBS (Benabid et al., 2009; Wichmann and Delong, 2006; but see Zaidel et al., 2010). Furthermore, one of the major effects of STh DBS is the reduction in required levodopa dose. Considering these observations and the relatively strong direct connections found earlier, one simple idea for the mechanism of DBS is the direct stimulation of residual dopamine neurons through direct activation of STh neuron axons, which, in turn, leads to the restoration of dopamine concentrations in target areas of SNc dopamine neurons (e.g., DS). Although earlier studies suggested ''inhibition'' of STh neurons by high-frequency stimulation may be the mechanism, recent studies have indicated that direct electrical stimulation of axons of STh neurons may actually cause an increase in the transmitter release at their target (Deniau et al., 2010; Johnson et al., 2008). Although whether STh DBS causes an increase in dopamine concentration remains controversial (Benazzouz et al., 2000; Hilker et al., 2003; Iribe et al., 1999; Nakajima et al., 2003; Pazo et al., 2010; Smith and Grace, 1992; Strafella et al., 2003), our study provides anatomical support for this model.

Interestingly, our results demonstrate that other targets of DBS also predominantly project directly to SNc dopamine neurons. These include the EP (homologous to the internal segment of the globus pallidus in humans), PTg, and motor cortex (Benabid et al., 2009; Wichmann and Delong, 2006). Although the relevance of these direct connections in DBS remains to be examined, cell-type-specific connectivity diagrams will aid future studies of the mechanisms as well as the search for new targets for DBS.

Future Directions

In the present study, we have focused on gross differences in inputs to VTA versus SNc dopamine neurons. Recent studies, however, have demonstrated more diversity in dopamine neurons than previously assumed (Ikemoto, 2007). For example, VTA dopamine neurons are composed of different subgroups that project to distinct areas, have distinct physiological properties, and involve distinct synaptic plasticity in response to cocaine and pain (Lammel et al., 2008; Lammel et al., 2011). It is thus of great interest to examine inputs to these subgroups separately.

Although VTA and SNc dopamine neurons have long been associated with different functions (e.g., reward and motor functions), it is only recently that the differences in firing patterns of VTA versus SNc dopamine neurons have been revealed (Matsumoto and Hikosaka, 2009). It is, therefore, important to replicate these results in different animals, including mice. Although response properties of dopamine neurons in awake-behaving mice have been relatively understudied, the availability of genetic and molecular tools can greatly facilitate detailed characterizations of midbrain dopamine neurons (Cohen et al., 2012). Furthermore, the present study revealed various direct inputs to dopamine neurons from relatively underappreciated areas such as motor, somatosensory, and autonomic areas. This knowledge will be useful in designing future recording experiments to probe further differences between VTA and SNc dopamine neurons.

EXPERIMENTAL PROCEDURES

Viral Injections

All procedures were approved by Harvard University Institutional Animal Care and Use Committee. Adult male mice (2 to 6 months old) were used. DAT-Cre (Bäckman et al., 2006) and Vgat-ires-Cre (Vong et al., 2011) lines were backcrossed with C57BL6. For some control experiments, C57BL6 mice were used. For cell-type-specific tracing, 0.1–0.5 μl of AAV8-FLEX-RG (2×10^{12} particles/ml) and AAV5-FLEX-TVA-mCherry (4×10^{12} particles/ml) were stereotaxically injected into the targeting areas using a micromanipulator with a pulled glass needle. Two weeks later, 4 μl of pseudotyped rabies virus, SADΔG-GFP(EnvA) (1.0×10^{7} plaque-forming units [pfu] per milliliter; Wickersham et al., 2007b), was injected into the same area. For tracing using the non-pseudotyped rabies virus, 4 μl of SADΔG-GFP (2×10^{8} pfu/ml) (Wickersham et al., 2007a) was injected into VTA. To directly compare the distributions of

neurons projecting to VTA versus SNc dopamine neurons, SADΔG-GFP(EnvA) (5×10^7 pfu/ml) and SADΔG-mCherry(EnvA) (1.0×10^6 pfu/ml) (Marshel et al., 2010) were injected at 3.0 mm posterior to Bregma, 4.2 mm deep from dura, 0.5 mm and 1.5 mm lateral to the midline, respectively.

Histology and Image Analysis

One week after injection of rabies virus, mice were perfused with PBS followed by 4% paraformaldehyde (PFA) in PBS. After 2 days of postfixation in 4% PFA, coronal brain slices at 100 μm thickness were prepared using a vibratome. Every third section was counterstained with NeuroTrace Fluorescent Nissl Stains (Molecular Probes, Eugene, OR, USA). Immunohistochemistry was performed using the anti-calbindin rabbit polyclonal antibodies (Calbiochem, Darmstadt, Germany), anti-tyrosine hydroxylase AB152 (Millipore, Billerica, MA, USA), the biotinylated goat anti-rabbit secondary antibodies (Jackson ImmunoResearch, West Grove, PA, USA), streptoavidin-conjugated Alexa Fluor 405, and Alexa Fluoro 594 goat anti-rabbit secondary antibodies (Molecular Probes). Slices were permeabilized with 0.5% Triton X-100, and incubation with antibodies and washing was done with 0.05% Triton X-100. Whole-section mosaics of high-magnification images were taken semiautomatically with AxioImager Z2 or LSM 510 Inverted Confocal microscopes (Zeiss) and assembled using software (Axiovision or LSM, Zeiss). The locations of labeled neurons and the outlines of brain areas were manually registered using custom software written in MATLAB (Mathworks, Natic, MA, USA). Further data analyses were performed using custom software written in MATLAB (see Supplemental Experimental Procedures).

SUPPLEMENTAL INFORMATION

Supplemental Information includes six figures and Supplemental Experimental Procedures and can be found with this article online at doi:10.1016/j.neuron.2012.03.017.

ACKNOWLEDGMENTS

We are grateful to Dr. Edward Callaway for providing us with the rabies virus and other reagents and his advice. We thank Dr. John A.T. Young for pCMMP-TVA950. We thank Dr. Catherine Dulac for her support, providing us with various reagents, and her comments on the manuscript. We thank Dr. Joshua Sanes for comments on the manuscript, Drs. Linh Vong and Bradford Lowell for Vgat-ires-Cre mouse, Dr. Edward Boyden for AAV8-CAG-ArchT-GFP, and Dr. Shenqin Yao for pCDNA-mCherry and her technical advice. We thank Neir Eshel, Jeremiah Cohen, and other members of the Uchida lab for critical comments on the manuscript and discussions. This work was supported by a Howard Hughes Medical Institute Collaborative Innovation Award, a Smith Family New Investigator Award, the Alfred Sloan Foundation, and the Milton Fund (N.U.).

Accepted: March 10, 2012
Published: June 6, 2012

REFERENCES

Bäckman, C.M., Malik, N., Zhang, Y., Shan, L., Grinberg, A., Hoffer, B.J., Westphal, H., and Tomac, A.C. (2006). Characterization of a mouse strain expressing Cre recombinase from the 3′ untranslated region of the dopamine transporter locus. Genesis *44*, 383–390.

Benabid, A.L., Chabardes, S., Mitrofanis, J., and Pollak, P. (2009). Deep brain stimulation of the subthalamic nucleus for the treatment of Parkinson's disease. Lancet Neurol. *8*, 67–81.

Benazzouz, A., Gao, D., Ni, Z., and Benabid, A.L. (2000). High frequency stimulation of the STN influences the activity of dopamine neurons in the rat. Neuroreport *11*, 1593–1596.

Berger, B., Gaspar, P., and Verney, C. (1991). Dopaminergic innervation of the cerebral cortex: unexpected differences between rodents and primates. Trends Neurosci. *14*, 21–27.

Bolam, J.P., and Smith, Y. (1990). The GABA and substance P input to dopaminergic neurones in the substantia nigra of the rat. Brain Res. *529*, 57–78.

Brischoux, F., Chakraborty, S., Brierley, D.I., and Ungless, M.A. (2009). Phasic excitation of dopamine neurons in ventral VTA by noxious stimuli. Proc. Natl. Acad. Sci. USA *106*, 4894–4899.

Brog, J.S., Salyapongse, A., Deutch, A.Y., and Zahm, D.S. (1993). The patterns of afferent innervation of the core and shell in the "accumbens" part of the rat ventral striatum: immunohistochemical detection of retrogradely transported fluoro-gold. J. Comp. Neurol. *338*, 255–278.

Bromberg-Martin, E.S., Matsumoto, M., and Hikosaka, O. (2010). Dopamine in motivational control: rewarding, aversive, and alerting. Neuron *68*, 815–834.

Bunney, B.S., and Aghajanian, G.K. (1976). The precise localization of nigral afferents in the rat as determined by a retrograde tracing technique. Brain Res. *117*, 423–435.

Burton, M.J., Rolls, E.T., and Mora, F. (1976). Effects of hunger on the responses of neurons in the lateral hypothalamus to the sight and taste of food. Exp. Neurol. *51*, 668–677.

Callaway, E.M. (2008). Transneuronal circuit tracing with neurotropic viruses. Curr. Opin. Neurobiol. *18*, 617–623.

Carr, D.B., and Sesack, S.R. (2000). Projections from the rat prefrontal cortex to the ventral tegmental area: target specificity in the synaptic associations with mesoaccumbens and mesocortical neurons. J. Neurosci. *20*, 3864–3873.

Chuhma, N., Tanaka, K.F., Hen, R., and Rayport, S. (2011). Functional connectome of the striatal medium spiny neuron. J. Neurosci. *31*, 1183–1192.

Cohen, J.Y., Haesler, S., Vong, L., Lowell, B.B., and Uchida, N. (2012). Neuron-type-specific signals for reward and punishment in the ventral tegmental area. Nature *482*, 85–88.

Coizet, V., Dommett, E.J., Klop, E.M., Redgrave, P., and Overton, P.G. (2010). The parabrachial nucleus is a critical link in the transmission of short latency nociceptive information to midbrain dopaminergic neurons. Neuroscience *168*, 263–272.

Collingridge, G.L., and Davies, J. (1981). The influence of striatal stimulation and putative neurotransmitters on identified neurones in the rat substantia nigra. Brain Res. *212*, 345–359.

DeFalco, J., Tomishima, M., Liu, H., Zhao, C., Cai, X., Marth, J.D., Enquist, L., and Friedman, J.M. (2001). Virus-assisted mapping of neural inputs to a feeding center in the hypothalamus. Science *291*, 2608–2613.

Deniau, J.M., Degos, B., Bosch, C., and Maurice, N. (2010). Deep brain stimulation mechanisms: beyond the concept of local functional inhibition. Eur. J. Neurosci. *32*, 1080–1091.

Dommett, E., Coizet, V., Blaha, C.D., Martindale, J., Lefebvre, V., Walton, N., Mayhew, J.E., Overton, P.G., and Redgrave, P. (2005). How visual stimuli activate dopaminergic neurons at short latency. Science *307*, 1476–1479.

Doya, K. (1999). What are the computations of the cerebellum, the basal ganglia and the cerebral cortex? Neural Netw. *12*, 961–974.

Franklin, B.J., and Paxinos, G. (2008). The mouse brain in stereotaxic coordinates. Compact third eddition (San Diego, CA: Academic Press).

Fujiyama, F., Sohn, J., Nakano, T., Furuta, T., Nakamura, K.C., Matsuda, W., and Kaneko, T. (2011). Exclusive and common targets of neostriatofugal projections of rat striosome neurons: a single neuron-tracing study using a viral vector. Eur. J. Neurosci. *33*, 668–677.

Futami, T., Takakusaki, K., and Kitai, S.T. (1995). Glutamatergic and cholinergic inputs from the pedunculopontine tegmental nucleus to dopamine neurons in the substantia nigra pars compacta. Neurosci. Res. *21*, 331–342.

Gauriau, C., and Bernard, J.F. (2002). Pain pathways and parabrachial circuits in the rat. Exp. Physiol. *87*, 251–258.

Geisler, S., and Zahm, D.S. (2005). Afferents of the ventral tegmental area in the rat-anatomical substratum for integrative functions. J. Comp. Neurol. *490*, 270–294.

Geisler, S., Derst, C., Veh, R.W., and Zahm, D.S. (2007). Glutamatergic afferents of the ventral tegmental area in the rat. J. Neurosci. *27*, 5730–5743.

Gerfen, C.R. (1984). The neostriatal mosaic: compartmentalization of corticostriatal input and striatonigral output systems. Nature *311*, 461–464.

Gerfen, C.R. (1992). The neostriatal mosaic: multiple levels of compartmental organization. Trends Neurosci. *15*, 133–139.

Gong, S., Doughty, M., Harbaugh, C.R., Cummins, A., Hatten, M.E., Heintz, N., and Gerfen, C.R. (2007). Targeting Cre recombinase to specific neuron populations with bacterial artificial chromosome constructs. J. Neurosci. *27*, 9817–9823.

Grace, A.A., and Bunney, B.S. (1985). Opposing effects of striatonigral feedback pathways on midbrain dopamine cell activity. Brain Res. *333*, 271–284.

Graybiel, A.M. (1990). Neurotransmitters and neuromodulators in the basal ganglia. Trends Neurosci. *13*, 244–254.

Graybiel, A.M., and Ragsdale, C.W., Jr. (1979). Fiber connections of the basal ganglia. Prog. Brain Res. *51*, 237–283.

Groenewegen, H.J., and Berendse, H.W. (1990). Connections of the subthalamic nucleus with ventral striatopallidal parts of the basal ganglia in the rat. J. Comp. Neurol. *294*, 607–622.

Haubensak, W., Kunwar, P.S., Cai, H., Ciocchi, S., Wall, N.R., Ponnusamy, R., Biag, J., Dong, H.W., Deisseroth, K., Callaway, E.M., et al. (2010). Genetic dissection of an amygdala microcircuit that gates conditioned fear. Nature *468*, 270–276.

Hilker, R., Voges, J., Ghaemi, M., Lehrke, R., Rudolf, J., Koulousakis, A., Herholz, K., Wienhard, K., Sturm, V., and Heiss, W.D. (2003). Deep brain stimulation of the subthalamic nucleus does not increase the striatal dopamine concentration in parkinsonian humans. Mov. Disord. *18*, 41–48.

Houk, J.C., Adams, J.L., and Barto, A.G. (1996). A model of how the basal ganglia generate and use neural signals that predict reinforcement, J.C. Houk, J.L. Davis, and D.G. Beiser, eds. (Cambridge, MA: The MIT Press).

Ikemoto, S. (2007). Dopamine reward circuitry: two projection systems from the ventral midbrain to the nucleus accumbens-olfactory tubercle complex. Brain Res. Brain Res. Rev. *56*, 27–78.

Iribe, Y., Moore, K., Pang, K.C., and Tepper, J.M. (1999). Subthalamic stimulation-induced synaptic responses in substantia nigra pars compacta dopaminergic neurons in vitro. J. Neurophysiol. *82*, 925–933.

Isoda, M., and Hikosaka, O. (2008). Role for subthalamic nucleus neurons in switching from automatic to controlled eye movement. J. Neurosci. *28*, 7209–7218.

Jackson, A., and Crossman, A.R. (1983). Nucleus tegmenti pedunculopontinus: efferent connections with special reference to the basal ganglia, studied in the rat by anterograde and retrograde transport of horseradish peroxidase. Neuroscience *10*, 725–765.

Jhou, T.C., Fields, H.L., Baxter, M.G., Saper, C.B., and Holland, P.C. (2009). The rostromedial tegmental nucleus (RMTg), a GABAergic afferent to midbrain dopamine neurons, encodes aversive stimuli and inhibits motor responses. Neuron *61*, 786–800.

Jin, X., and Costa, R.M. (2010). Start/stop signals emerge in nigrostriatal circuits during sequence learning. Nature *466*, 457–462.

Joel, D., and Weiner, I. (2000). The connections of the dopaminergic system with the striatum in rats and primates: an analysis with respect to the functional and compartmental organization of the striatum. Neuroscience *96*, 451–474.

Joel, D., Niv, Y., and Ruppin, E. (2002). Actor-critic models of the basal ganglia: new anatomical and computational perspectives. Neural Netw. *15*, 535–547.

Johnson, M.D., Miocinovic, S., McIntyre, C.C., and Vitek, J.L. (2008). Mechanisms and targets of deep brain stimulation in movement disorders. Neurotherapeutics *5*, 294–308.

Joshua, M., Adler, A., Mitelman, R., Vaadia, E., and Bergman, H. (2008). Midbrain dopaminergic neurons and striatal cholinergic interneurons encode the difference between reward and aversive events at different epochs of probabilistic classical conditioning trials. J. Neurosci. *28*, 11673–11684.

Kawato, M., and Samejima, K. (2007). Efficient reinforcement learning: computational theories, neuroscience and robotics. Curr. Opin. Neurobiol. *17*, 205–212.

Kita, H., and Kitai, S.T. (1987). Efferent projections of the subthalamic nucleus in the rat: light and electron microscopic analysis with the PHA-L method. J. Comp. Neurol. *260*, 435–452.

Lammel, S., Hetzel, A., Häckel, O., Jones, I., Liss, B., and Roeper, J. (2008). Unique properties of mesoprefrontal neurons within a dual mesocorticolimbic dopamine system. Neuron *57*, 760–773.

Lammel, S., Ion, D.I., Roeper, J., and Malenka, R.C. (2011). Projection-specific modulation of dopamine neuron synapses by aversive and rewarding stimuli. Neuron *70*, 855–862.

Lee, C.R., and Tepper, J.M. (2009). Basal ganglia control of substantia nigra dopaminergic neurons. J. Neural Transm. Suppl. *73*, 71–90.

Lévesque, M., and Parent, A. (2005). The striatofugal fiber system in primates: a reevaluation of its organization based on single-axon tracing studies. Proc. Natl. Acad. Sci. USA *102*, 11888–11893.

Lokwan, S.J., Overton, P.G., Berry, M.S., and Clark, D. (1999). Stimulation of the pedunculopontine tegmental nucleus in the rat produces burst firing in A9 dopaminergic neurons. Neuroscience *92*, 245–254.

Lynd-Balta, E., and Haber, S.N. (1994). The organization of midbrain projections to the ventral striatum in the primate. Neuroscience *59*, 609–623.

Marshel, J.H., Mori, T., Nielsen, K.J., and Callaway, E.M. (2010). Targeting single neuronal networks for gene expression and cell labeling in vivo. Neuron *67*, 562–574.

Matsumoto, M., and Hikosaka, O. (2007). Lateral habenula as a source of negative reward signals in dopamine neurons. Nature *447*, 1111–1115.

Matsumoto, M., and Hikosaka, O. (2009). Two types of dopamine neuron distinctly convey positive and negative motivational signals. Nature *459*, 837–841.

Matsumura, M., Kojima, J., Gardiner, T.W., and Hikosaka, O. (1992). Visual and oculomotor functions of monkey subthalamic nucleus. J. Neurophysiol. *67*, 1615–1632.

Miyamichi, K., Amat, F., Moussavi, F., Wang, C., Wickersham, I., Wall, N.R., Taniguchi, H., Tasic, B., Huang, Z.J., He, Z., et al. (2011). Cortical representations of olfactory input by trans-synaptic tracing. Nature *472*, 191–196.

Naito, A., and Kita, H. (1994). The cortico-pallidal projection in the rat: an anterograde tracing study with biotinylated dextran amine. Brain Res. *653*, 251–257.

Nakajima, T., Nimura, T., Yamaguchi, K., Ando, T., Itoh, M., Yoshimoto, T., and Shirane, R. (2003). The impact of stereotactic pallidal surgery on the dopamine D2 receptor in Parkinson disease: a positron emission tomography study. J. Neurosurg. *98*, 57–63.

Nambu, A., Tokuno, H., and Takada, M. (2002). Functional significance of the cortico-subthalamo-pallidal 'hyperdirect' pathway. Neurosci. Res. *43*, 111–117.

Oakman, S.A., Faris, P.L., Kerr, P.E., Cozzari, C., and Hartman, B.K. (1995). Distribution of pontomesencephalic cholinergic neurons projecting to substantia nigra differs significantly from those projecting to ventral tegmental area. J. Neurosci. *15*, 5859–5869.

Okada, K., Toyama, K., Inoue, Y., Isa, T., and Kobayashi, Y. (2009). Different pedunculopontine tegmental neurons signal predicted and actual task rewards. J. Neurosci. *29*, 4858–4870.

Omelchenko, N., Bell, R., and Sesack, S.R. (2009). Lateral habenula projections to dopamine and GABA neurons in the rat ventral tegmental area. Eur. J. Neurosci. *30*, 1239–1250.

Omelchenko, N., and Sesack, S.R. (2010). Periaqueductal gray afferents synapse onto dopamine and GABA neurons in the rat ventral tegmental area. J. Neurosci. Res. *88*, 981–991.

Ono, T., Nakamura, K., Nishijo, H., and Fukuda, M. (1986). Hypothalamic neuron involvement in integration of reward, aversion, and cue signals. J. Neurophysiol. *56*, 63–79.

Pazo, J.H., Höcht, C., Barceló, A.C., Fillipini, B., and Lomastro, M.J. (2010). Effect of electrical and chemical stimulation of the subthalamic nucleus on the release of striatal dopamine. Synapse *64*, 905–915.

Peciña, S., and Berridge, K.C. (2005). Hedonic hot spot in nucleus accumbens shell: where do mu-opioids cause increased hedonic impact of sweetness? J. Neurosci. *25*, 11777–11786.

Phillipson, O.T. (1979). Afferent projections to the ventral tegmental area of Tsai and interfascicular nucleus: a horseradish peroxidase study in the rat. J. Comp. Neurol. *187*, 117–143.

Redgrave, P., and Gurney, K. (2006). The short-latency dopamine signal: a role in discovering novel actions? Nat. Rev. Neurosci. *7*, 967–975.

Saper, C.B. (2002). The central autonomic nervous system: conscious visceral perception and autonomic pattern generation. Annu. Rev. Neurosci. *25*, 433–469.

Saper, C.B. (2004). Central autonomic system, G. Paxinos, ed. (San Diego, CA: Academic Press), pp. 761–796.

Scarnati, E., Campana, E., and Pacitti, C. (1984). Pedunculopontine-evoked excitation of substantia nigra neurons in the rat. Brain Res. *304*, 351–361.

Schultz, W. (2007). Multiple dopamine functions at different time courses. Annu. Rev. Neurosci. *30*, 259–288.

Schultz, W., Dayan, P., and Montague, P.R. (1997). A neural substrate of prediction and reward. Science *275*, 1593–1599.

Sesack, S.R., and Grace, A.A. (2010). Cortico-basal ganglia reward network: microcircuitry. Neuropsychopharmacology *35*, 27–47.

Smith, I.D., and Grace, A.A. (1992). Role of the subthalamic nucleus in the regulation of nigral dopamine neuron activity. Synapse *12*, 287–303.

Smith, Y., Hazrati, L.N., and Parent, A. (1990). Efferent projections of the subthalamic nucleus in the squirrel monkey as studied by the PHA-L anterograde tracing method. J. Comp. Neurol. *294*, 306–323.

Somogyi, P., Bolam, J.P., Totterdell, S., and Smith, A.D. (1981). Monosynaptic input from the nucleus accumbens—ventral striatum region to retrogradely labelled nigrostriatal neurones. Brain Res. *217*, 245–263.

Strafella, A.P., Sadikot, A.F., and Dagher, A. (2003). Subthalamic deep brain stimulation does not induce striatal dopamine release in Parkinson's disease. Neuroreport *14*, 1287–1289.

Suri, R.E. (2002). TD models of reward predictive responses in dopamine neurons. Neural Netw. *15*, 523–533.

Swanson, L.W. (2000). Cerebral hemisphere regulation of motivated behavior. Brain Res. *886*, 113–164.

Ugolini, G. (2011). Rabies virus as a transneuronal tracer of neuronal connections. Adv. Virus Res. *79*, 165–202.

Vong, L., Ye, C., Yang, Z., Choi, B., Chua, S., Jr., and Lowell, B.B. (2011). Leptin action on GABAergic neurons prevents obesity and reduces inhibitory tone to POMC neurons. Neuron *71*, 142–154.

Wall, N.R., Wickersham, I.R., Cetin, A., De La Parra, M., and Callaway, E.M. (2010). Monosynaptic circuit tracing in vivo through Cre-dependent targeting and complementation of modified rabies virus. Proc. Natl. Acad. Sci. USA *107*, 21848–21853.

Wichmann, T., and Delong, M.R. (2006). Deep brain stimulation for neurologic and neuropsychiatric disorders. Neuron *52*, 197–204.

Wickersham, I.R., Finke, S., Conzelmann, K.K., and Callaway, E.M. (2007a). Retrograde neuronal tracing with a deletion-mutant rabies virus. Nat. Methods *4*, 47–49.

Wickersham, I.R., Lyon, D.C., Barnard, R.J., Mori, T., Finke, S., Conzelmann, K.K., Young, J.A., and Callaway, E.M. (2007b). Monosynaptic restriction of transsynaptic tracing from single, genetically targeted neurons. Neuron *53*, 639–647.

Wise, R.A. (2004). Dopamine, learning and motivation. Nat. Rev. Neurosci. *5*, 483–494.

Xia, Y., Driscoll, J.R., Wilbrecht, L., Margolis, E.B., Fields, H.L., and Hjelmstad, G.O. (2011). Nucleus accumbens medium spiny neurons target non-dopaminergic neurons in the ventral tegmental area. J. Neurosci. *31*, 7811–7816.

Yamamoto, T. (2006). Neural substrates for the processing of cognitive and affective aspects of taste in the brain. Arch. Histol. Cytol. *69*, 243–255.

Yoon, H., Enquist, L.W., and Dulac, C. (2005). Olfactory inputs to hypothalamic neurons controlling reproduction and fertility. Cell *123*, 669–682.

Zahm, D.S., and Brog, J.S. (1992). On the significance of subterritories in the "accumbens" part of the rat ventral striatum. Neuroscience *50*, 751–767.

Zahm, D.S., Cheng, A.Y., Lee, T.J., Ghobadi, C.W., Schwartz, Z.M., Geisler, S., Parsely, K.P., Gruber, C., and Veh, R.W. (2011). Inputs to the midbrain dopaminergic complex in the rat, with emphasis on extended amygdala-recipient sectors. J. Comp. Neurol. *519*, 3159–3188.

Zaidel, A., Bergman, H., Ritov, Y., and Israel, Z. (2010). Levodopa and subthalamic deep brain stimulation responses are not congruent. Mov. Disord. *25*, 2379–2386.

Neuron, Volume *74*

Supplemental Information

Whole-Brain Mapping of Direct Inputs to Midbrain Dopamine Neurons

Mitsuko Watabe-Uchida, Lisa Zhu, Sachie K. Ogawa, Archana Vamanrao, and Naoshige Uchida

INVENTORY OF SUPPLEMENTAL INFORMATION

SUPPLEMENTAL FIGURES

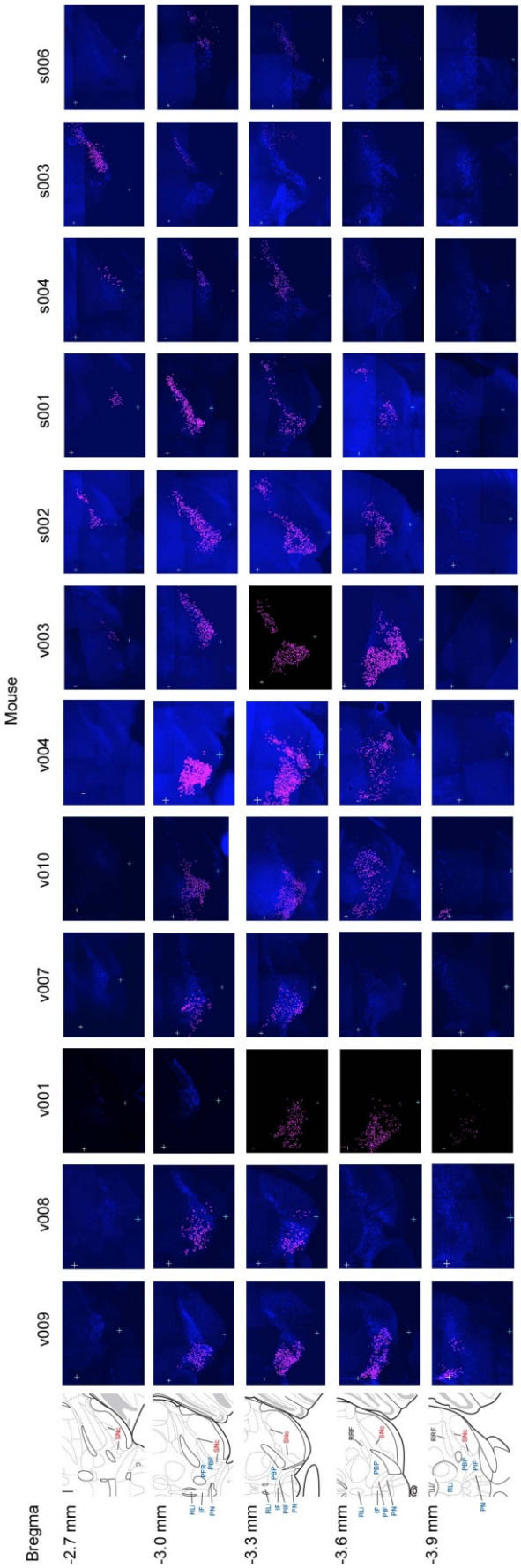

Figure S1. Distribution of starter neurons

Starter neurons (magenta) are plotted on five coronal sections. Sections were immunostained for TH (blue) except for v001. The reference atlas (Left) is from Franklin and Paxinos (2008). White crosses, midline. Cyan crosses,1 mm lateral to midline.

IF: interfascicular nucleus, PBP: parabrachial pigmented nucleus of VTA, PFR: parafasciclus retroflexus area, PIF: parainterfascicular nucleus of VTA, PN: paranigral nucleus of VTA, RLi: rostral linear nucleus, RRF: retrorubral field (A8).

Note that the IF, PBP, PFR, PIF, PN and RLi constitute the VTA or A10 (Ikemoto, 2007). In Franklin and Paxinos (2008), the VTA refers to PFR only.

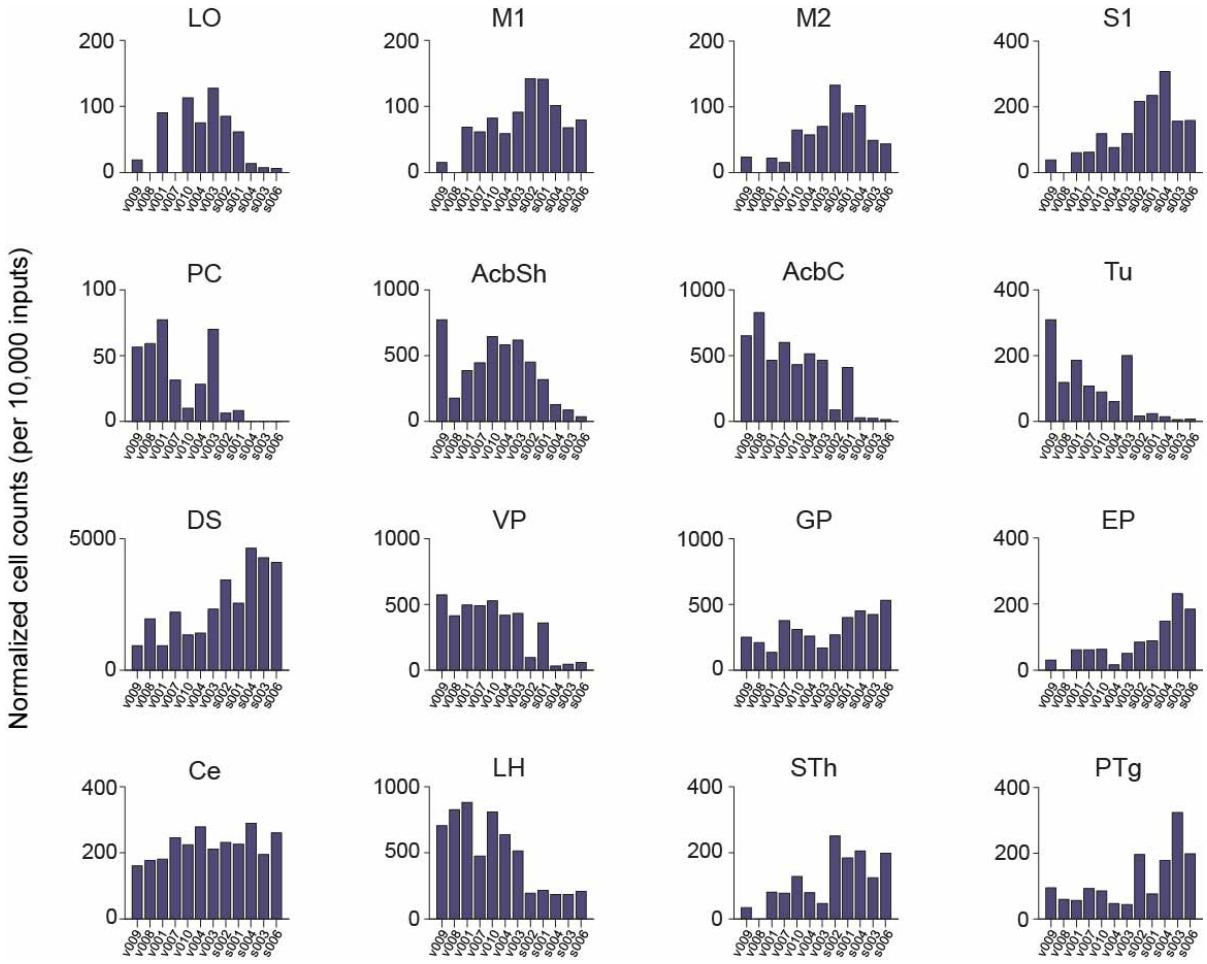

Figure S2. Cell counts from individual animals

LO, lateral orbital cortex; M1, primary motor cortex; M2, secondary motor cortex; S1, primary somatosensory cortex; PC, piriform cortex; AcbSh, nucleus accumbens shell; AcbC, nucleus accumbens core; Tu, olfactory tubercle; DS, dorsal striatum; VP, ventral pallidum; GP, globus pallidus; EP, entopeduncular nucleus; Ce, central nucleus of the amygdala; LH, lateral hypothalamus; STh, subthalamic nucleus; PTg, pedunculotegmental nucleus.

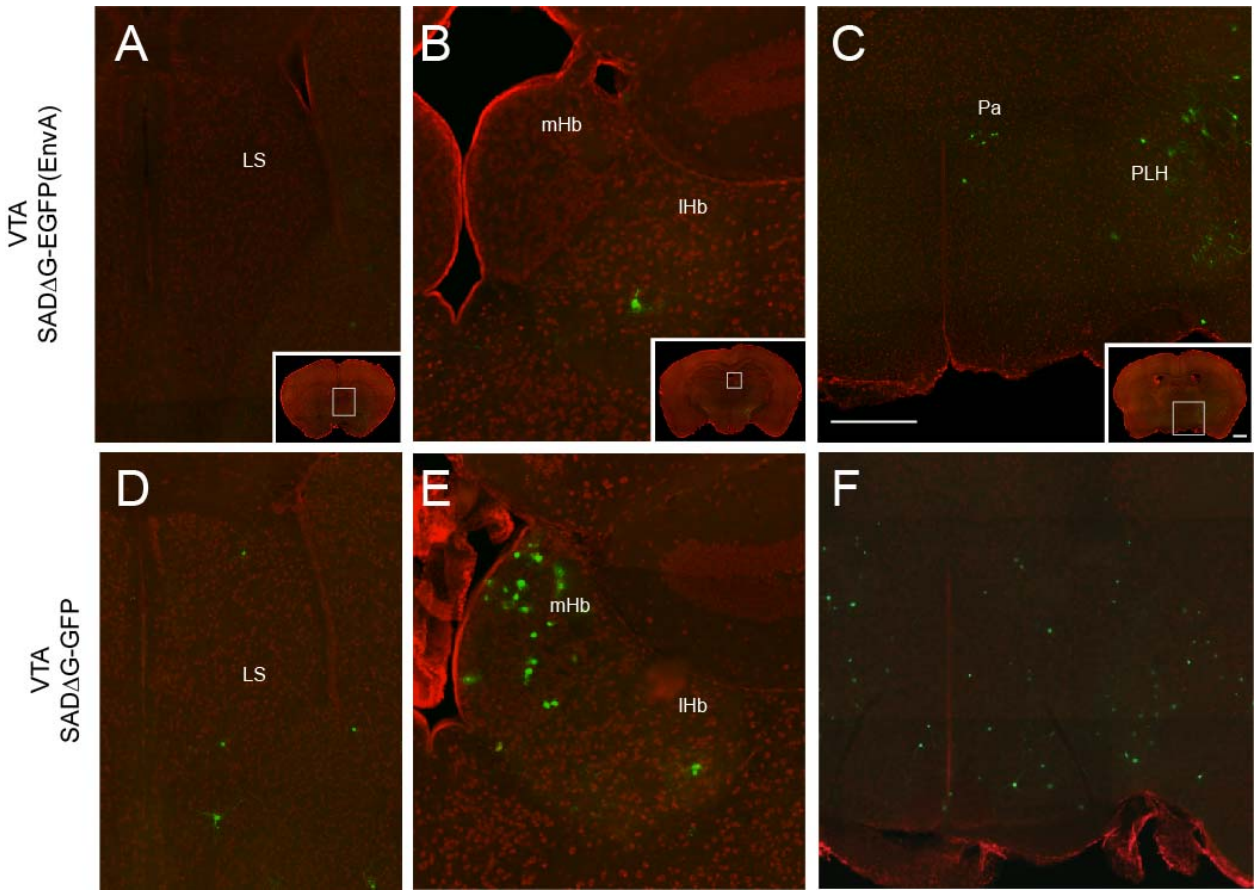

Figure S3. Comparison between tracing using Cre-dependent, transsynaptic tracing and Cre-independent, non-transsynaptic tracing.

(A, D) Lateral septum (LS)

(B, E) Medial and lateral habenula (mHb and lHb).

(C, F) Hypothalamic areas. Pa, paraventricular hypothalamic nucleus; PLH, peduncular part of the lateral hypothalamus (LH).

The EGFP patterns with selective tracing using SADdG-GFP(envA) in DAT-Cre mice (A-C) are compared with those with nonselective tracing using unpseudotyped SADdG-GFP (D-F). Green, EGFP expressed by rabies virus; red, fluorescent Nissl staining. Insets show low magnification views of sections. The white rectangles indicate the magnified regions. Scale bars, 250 μm and 1 mm (insets). Significantly more labeling is observed with nonspecific tracing in LS (D) and mHb (E) compared to the tracing with DAT-Cre mice. In the hypothalamus, Pa and LH showed prominent labeling with DAT-Cre mice (C) while more widespread labeling was observed with nonspecific tracing (F).

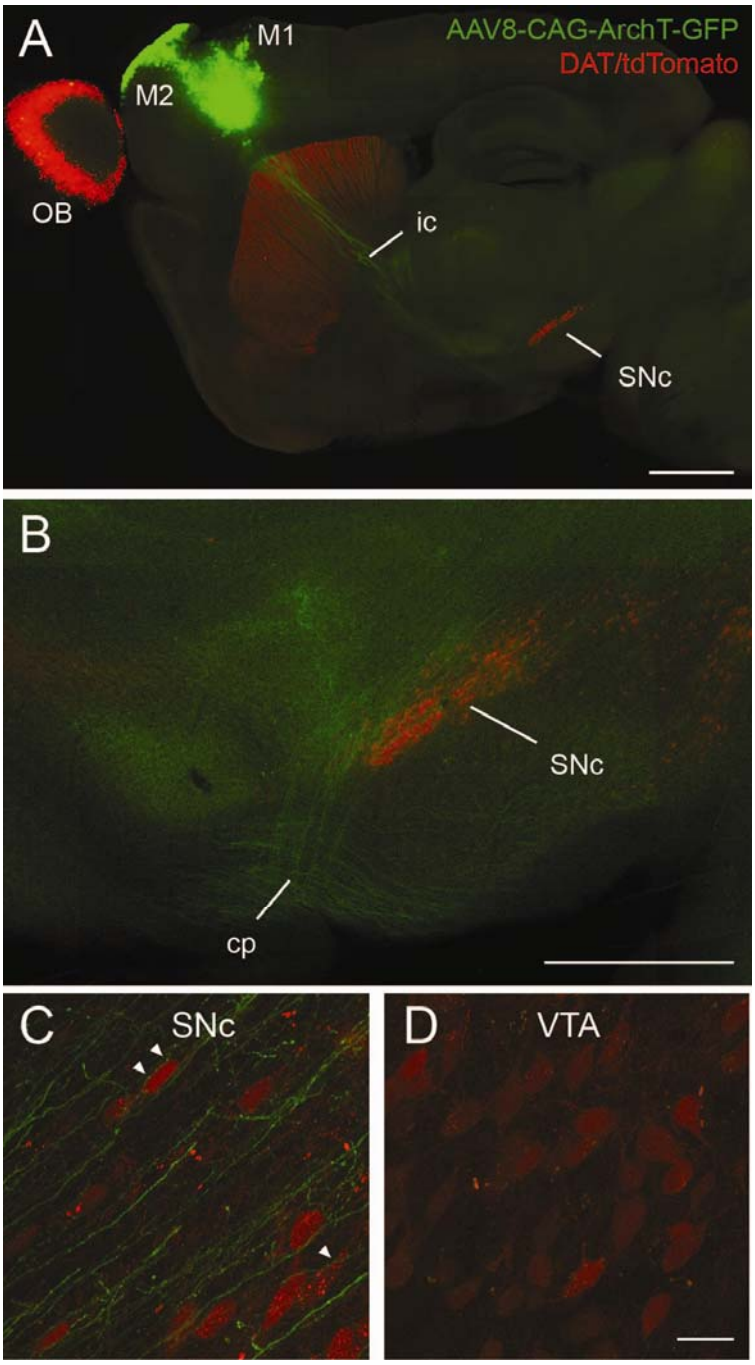

Figure S4. Anterograde tracing from the motor cortex.

(A) A low magnification view of a sagittal section. AAV8-CAG-ArchT-GFP was injected into the motor cortex. The mouse expresses tdTomato in dopamine neurons. Green: AAV8-CAG-ArchT-GFP. Red: tdTomato. Strong signals in the olfactory bulb (OB) reflect dopaminergic interneurons. Scales bar: 1 mm.

(B) A medium magnification view near SNc. Scale bar: 500 μm.

(C) A high magnification view of SNc. Arrowheads indicate buttons.

(D) A high magnification view of VTA. Scale bar: 20 μm.

cp: cortical peduncle. ic: internal capusule. OB: olfactory bulb. M1: primary motor cortex. M2: secondary motor cortex.

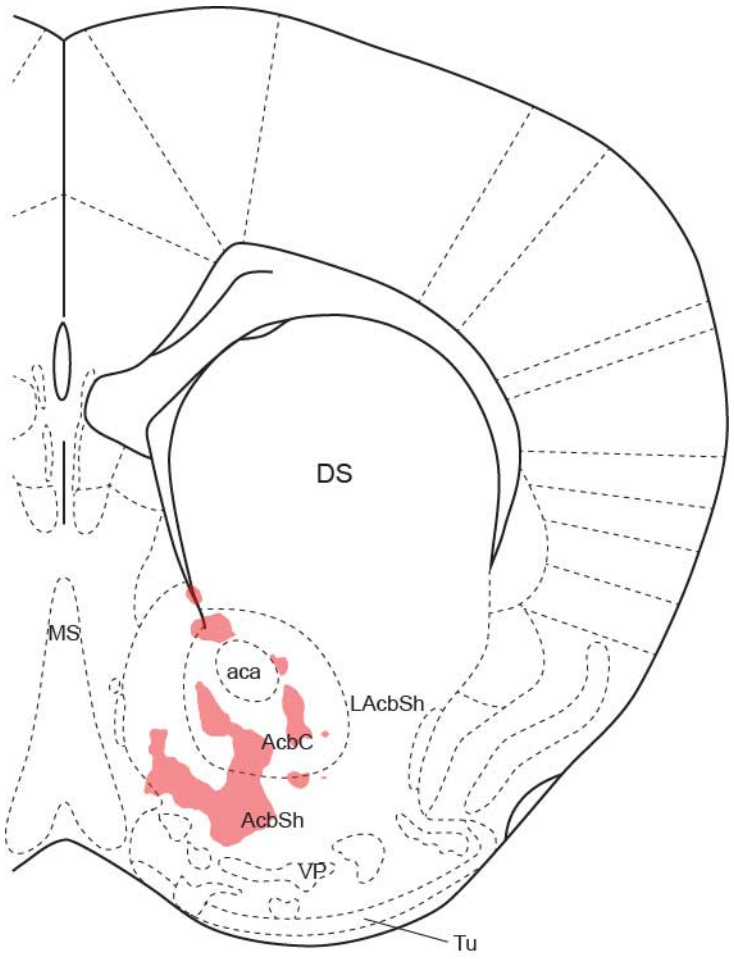

Figure S5. Patterns of dopamine neuron-projecting "ventral patches" in the nucleus accumbens.

The average patch patterns are obtained from 5 VTA-targeted mice. The atlas is after Franklin and Paxinos (2008). MS, medial septal nucleus; aca, anterior part of anterior commissure; AcbC, nucleus accumbens core; AcbSh, nucleus accumbens shell; LAcbSh, lateral accumbens shell; DS, dorsal striatum; VP, ventral pallidum; Tu, olfactory tubercle.

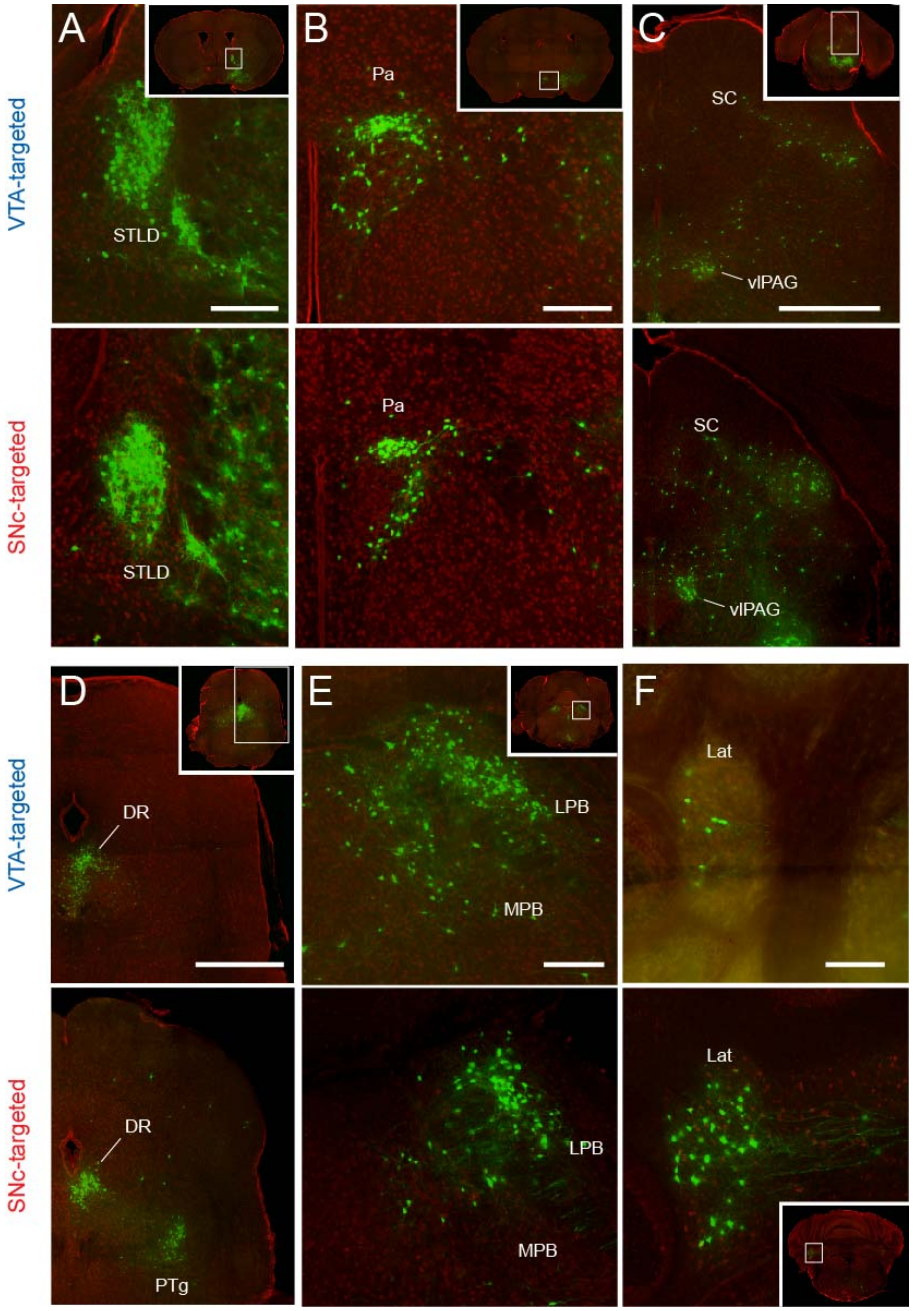

Figure S6. Comparisons of other major input areas

(A) Bed nucleus of stria terminalis (BNST). STLD, dorsal lateral division of the bed nucleus of stria terminalis.

(B) Paraventricular hypothalamic nucleus (Pa).

(C) Superior colliculus (SC) and periaqueductal gray (PAG). Dopamine projecting neurons are clustered in the ventrolateral part of the PAG (vlPAG).

(D) Dorsal raphe (DR) and pedunculotegmental nucleus (PTg).

(E) Parabrachial nucleus (PB). Both lateral and medial PB contains labeled neurons.

(F) Cerebellar nuclei. Lat, lateral (dentate) cerebellar nucleus.

Insets show low magnification views of sections. The white rectangles indicate the magnified regions. Scale bar, 1 mm (C, D) and 250 μm (A, B, E, F).

SUPPLEMENTAL EXPERIMENTAL PROCEDURES

Production of viral vectors

Different serotypes of AAVs and different promoters were used to express RG and TVA under the control of a FLEX switch (Atasoy et al., 2008), to avoid any possible competition. AAV8 and AAV5 were chosen due to the highest expression efficiency in midbrain dopamine neurons in the pilot experiments. To maximize the expression efficiency after Cre recombination, a FLEX switch was designed to contain lox2272 and loxP sites, oriented to have no false ATG start, with point mutations in the inverted repeats to destabilize hairpin structures in transcribed RNA as below. To generate a mammalian expression vector with the FLEX switch under chicken actin promoter, annealed oligonucleotides (Integrated DNA Technologies, Coralville, IA) were ligated between EcoRI and NheI sites of pCA-MCS (pCA-FLEX). CA-FLEX fragment, digested with SmaI and NheI and blunted by T4 DNA polymerase, was inserted at HindIII site, blunted and BamHI site into pAAV-DIO-hChR2EYFP (pAAV-CA-FLEX) (Gunaydin et al., 2010). Rabies glycoprotein ORF was obtained from pHCMV-RG (Sena-Esteves et al., 2004) by AseI/EcoRV digestion, blunted, and inserted at EcoRV site of pAAV-CA-FLEX (pAAV-CA-FLEX-RG).

FLEX:

GAATTCATtACcTCGTATAGGATACTTTATACGAAGTTATGCAGAATGGTAGCTGGATTGTAAGTACTA
TTAGCAATATGAAACCTCTTAATAACcTCGTATAGCATACATTATACGAAGTaATAGATCTAAGCTTGA
TATCGTCGACATAACTTCGTATAAAGTATCCTATACGAgGTaATTTGCCTTAACCCAGAAATTATCAGT
ACTATTCTTTAGAATGGTGCAAAGAATtACTTCGTATAATGTATGCTATACGAgGTTATCGCATGCTAG
C

A transmembrane version of TVA, TVA950 (Qin and Luo, 2009), was shuttled from pCMMP-TVA950 by PmlI/BamHI digestion at BamHI and EcoRV sites of pBluescriptII SK (pB-TVA950). mCherry open reading frame was amplified by PCR using pCDNA-mCherry and primers below, and inserted at StyI site blunted, and BamHI site of pB-TVA950 (pB-TVA950-mCherry). TVA950-mCherry fragment, digested with SalI and EcoRV and blunted, was inserted at NheI and AscI sites, blunted, of pAAV-DIO-hChR2EYFP (pAAV-EF1α-FLEX-TVA-mCherry).

mCherry-s: TTTTT CCC GGG GGT GGG GTG AGC AAG GGC GAG GAG G

mCherry-a: TTTTT GGATCC GAT ATC TTA CTT GTA CAG CTC GTC CA

AAV8-FLEX-RG and AAV5-FLEX-TVA-mCherry were produced by Virus Vector Core Facility of the University of North Carolina (Chapel Hill, NC). Pseudotyped and unpseudotyped rabies viruses were produced as described previously (Wickersham et al., 2010). Contamination of unpseudotyped virus was <1 in 10^4 pseudotyped virus using 293T cells.

Image analysis

The locations of labeled neurons and the outlines of brain areas were manually registered using custom software written in MATLAB (Mathworks, Natic, MA). In some cases, images were low-pass filtered using a Gaussian kernel before analysis. This reduced diffuse fluorescent signals originating from axon fibers and emphasized signals from somata. The nomenclatures and outlines of brain areas are according to a standard mouse atlas (Franklin and Paxinos, 2008). Abbreviations are also according to Franklin and Paxinos (2008) except we used the dorsal striatum (DS) instead of caudate/putamen (CPu). Note that the pedunculotegmental nucleus (PTg) is often called the pedunculopontine tegmental nucleus, and that the orbital cortex is often called the orbitofrontal cortex in other literature. The globus pallidus and entopeduncular nucleus in rodents are thought to be equivalent to the external segments and internal segments of the globus pallidus in primates, respectively. Numbers of neurons were normalized by the total number of input neurons in the entire brain of each animal. Because the numbers of input neurons are roughly proportional to those of starter neurons, both produce similar results. Because v008 and v007 contained relatively small numbers of transsynaptically labeled neurons (Figure 1F), the results from these mice were excluded from quantitative analysis. However, except some areas that contained a small number of input neurons, the results from these mice were consistent with other animals (Figure S2).

Center of mass analysis

To compare global shift of EGFP-positive neurons, the center of mass of a brain section was obtained by averaging positions of neurons. To superimpose results from different animals onto a standard atlas, neuron's positions were normalized by anatomical landmarks. For Figure 4A-C, we used the midline and the lateral most part of the dorsal striatum (DS). For Figure 4D-F, we used the midline and the medial most position of the cerebral peduncle (cp).

Analysis of the neocortex

Various efforts have been made to identify cortical areas in rodents. However, resulting maps differ significantly across studies (Plalomero-Gallagher and Zilles, 2004). We therefore examined distributions of the labeled neurons in the entire neocortex using an "unrolled map". To make an unrolled map, we first drew a line running at the middle of the cortical sheet (the gray lines in Figure 5C and F). For reference points, we used the most dorsomedial corner of the hemisphere (the black crosses in Figure 5C and F) and rhenal fissure or sulcus (red triangles). These reference points were projected onto the line (black dots and red crosses). These lines were "unrolled" and aligned according to the dorsomedial reference point and the rostro-caudal position in reference to the bregma (Figure 5G and H). This unrolled map allows one to compare results across studies independent from the discrepancies in cortical maps. For comparison, we generated a reference unrolled map according to a mouse standard atlas (Figure 5I) (Franklin and Paxinos, 2008).

For cell counting (Figure 3), areas in the neocortex were parceled mostly according to the proportions of cortical areas on the coronal slices in the standard atlas (Franklin and Paxinos, 2008). Slight changes in the locations of the boundaries of cortical areas do not significantly affect the results.

Analysis of striatal neurons

For the quantification of calbindin D-28k immunofluorescence, we normalized the pixel intensities by the maximum and minimum of the area of interest. For each neuron, intensities were obtained in a circular area with diameter 6.8 μm. For measuring soma sizes, a stack of confocal images was projected along the z-axis. The soma of each neuron was outlined using custom software written in MATLAB and the area within the contour was calculated. We then calculated the diameter based on the area assuming a circle.

For a measure of dendritic complexities (Figure 6K), dendrites were traced using custom software in MATLAB. Dendritic length is defined as the total length along the dendrite. Radial distance is defined as the straight line distance between the most proximal point of the dendrite and the tip of the dendrite.

To obtain standard "ventral patches", locations of labeled neurons from 5 VTA-targeted mice were pooled. The data from different animals were combined using a normalized coordinate using the midline and the anterior commissure (the cross in Figure 7) as the reference points. The information about the locations of labeled neurons was "smoothed" by a circular averaging filter of the radius of 0.08 mm to obtain a density map. A contour line was drawn at half of the maximum density. To test the conservation of the location of the patches, "predicted" contour maps were obtained for each animal using data from the other 4 animals (one-leave-out cross-validation method) and the proportion of the neurons within the contour lines (patches) against the total number in Acb was calculated ("% neurons in predicted contours"). We then tested whether this value is larger than the proportion of the areas of the patches compared to that of the Acb (paired t-test).

Anterograde labeling from the motor cortex

To confirm projections from the motor cortex to SNc dopamine neurons, AAV8-CAG-ArchT-GFP (1.3×10^{11} particles/ml, a gift from Dr. Edward Boyden, generated by UNC Virus Vector Core Facility, Chapel Hill, NC) was injected into the motor cortex (bregma: +2.0 mm, 1.3 mm lateral from the midline) in two mice. We used DAT-Cre/Gt(ROSA)26 $^{Sortm(CAG-tdTomato)Hze}$ (Jackson Lab, Bar Harbor, ME) to label dopamine neurons with a fluorescent marker, tdTomato. After 17 days from injection, mice were perfused with 4% paraformaldehyde, and 100 μm sagittal sections were cut for observation (Figure S4).

SUPPLEMENTAL REFERENCES

Atasoy, D., Aponte, Y., Su, H.H., and Sternson, S.M. (2008). A FLEX switch targets Channelrhodopsin-2 to multiple cell types for imaging and long-range circuit mapping. J Neurosci *28*, 7025-7030.

Franklin, B.J., and Paxinos, G. (2008). The mouse brain in stereotaxic coordinates. Compact third eddition. (San Diego, Academic Press).

Gunaydin, L.A., Yizhar, O., Berndt, A., Sohal, V.S., Deisseroth, K., and Hegemann, P. (2010). Ultrafast optogenetic control. Nat Neurosci *13*, 387-392.

Plalomero-Gallagher, N., and Zilles, K. (2004). Isocortex. In The rat nervous system, Third edition, G. Paxinos, ed. (San Diego, Academic Press), pp. 729-757.

Qin, C., and Luo, M. (2009). Neurochemical phenotypes of the afferent and efferent projections of the mouse medial habenula. Neuroscience *161*, 827-837.

Sena-Esteves, M., Tebbets, J.C., Steffens, S., Crombleholme, T., and Flake, A.W. (2004). Optimized large-scale production of high titer lentivirus vector pseudotypes. J Virol Methods *122*, 131-139.

Wickersham, I.R., Sullivan, H.A., and Seung, H.S. (2010). Production of glycoprotein-deleted rabies viruses for monosynaptic tracing and high-level gene expression in neurons. Nat Protoc *5*, 595-606.